Student Friendly Guide

to the

Cosmic Microwave Background

Robert D. Klauber

Abstract

This document provides what is hopefully a relatively easy-to-understand introduction, suitable for someone with undergraduate physics training, to the power spectral analysis of the cosmic microwave background (CMB), as unveiled by the COBE, WMAP, Planck and other experiments of the past two decades. It proceeds step-by-small-step at a moderate (by physics standards) level of mathematical sophistication, and can serve as a simplified initial foundation for those wishing to enter the field, or for others who simply desire a more in-depth understanding of the CMB than the online popular accounts offer. It is half way between those online popularizations and typical cosmology textbooks.

Full disclosure

I am not a researcher/expert in this topic, but feel I can offer a fair pedagogic introduction to some areas of the subject for others like me who have physics backgrounds, but are not working in the field. Suggestions and corrections are always welcome via the feedback link on the home page above (which also contains links to pedagogic treatments of other physics topics).

RDK

Two Parts to This Document

This document is divided into two main parts, the basic introduction and the appendices. The basic material covers the physical mechanisms giving rise to the cosmic microwave background (CMB) and how we analyze the CMB using spherical harmonics. The appendices provide a fairly in depth development of spherical harmonic analysis and power spectral analysis, for those not completely at home with them. The first part comprises 23 pages; the appendices, 17 pages.

Table of Contents

Part 1

Part 2

1 The Cosmic Microwave Background Power Spectrum

If you are reading this, you have no doubt seen the diagram of Fig. 1. It shows the now famous cosmic microwave background (CMB) power spectral analysis of temperature variations across our sky. In this document, I try to present an introduction to it (where it comes from, what is the math behind it, and what it means) that is reasonably transparent to anyone with an undergraduate background in physics.
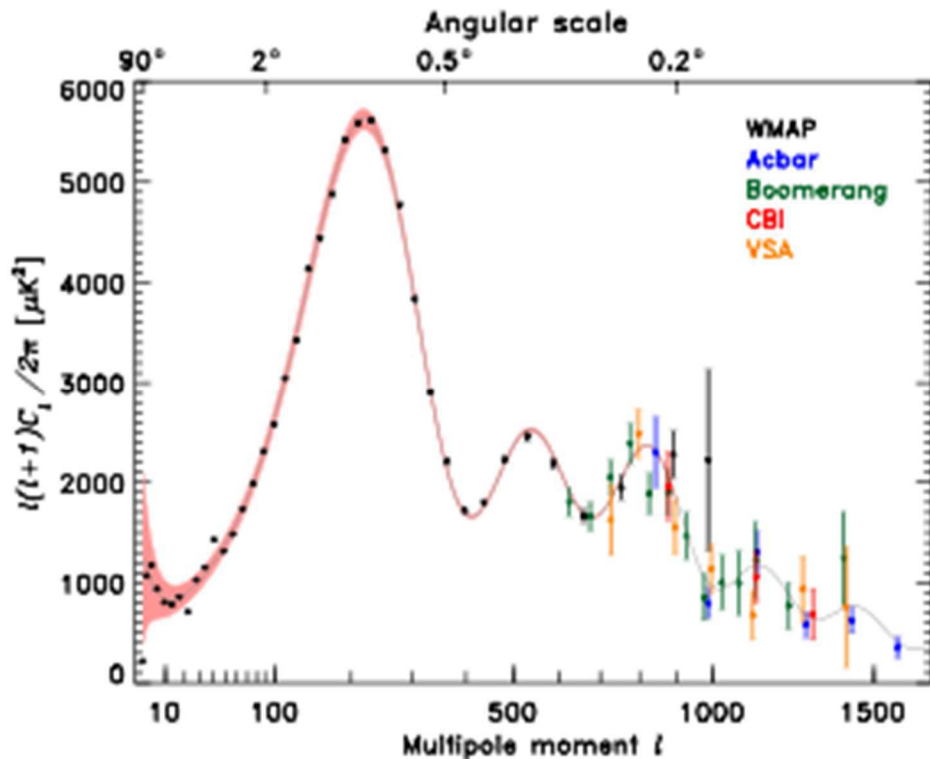

Figure 1. Power Spectrum of the Cosmic Microwave Background Variations

[Added May 15, 2019 →] The CMB today makes up 99.99% of all radiation in the universe.

2 Spatial Temperature Variations from Early Quantum Fluctuations

In this section, we do a brief overview of where the temperature variations of the cosmic microwave background (CMB) come from.

2.1 Traveling Pressure (Acoustic) Waves from Quantum Fluctuations

Tiny spatial variations in one or more quantum fields right after the big bang lead to spatial variations in mass-energy density. These variations grow to macroscopic scales via inflation and the subsequent expansion of the universe. Such variations comprise regions of greater mass-energy density and regions of lesser mass-energy density. The denser regions attract other matter and initially the dense regions grow denser and the rarefied regions grow more rarefied. This process would simply continue except that a pressure develops in the denser regions that begins to repel the matter moving toward them. The pressure arises as follows.

For the first 380,000 or so years after the big bang, temperature was so high that atoms could not form, and the universe consisted of a "soup" (a plasma really) of elementary particles interacting with one another. The primary interactions were electromagnetic ones between charged baryons and photons, which were continually and frenetically bouncing off one another. Thus, the photons exert a pressure on the baryons. If mass-energy were distributed completely evenly, the pressure, as in a static perfect fluid, would be the same everywhere.

However, as the denser regions attract mass-energy (baryons and photons) from the less dense regions, the e/m interactions in the denser region increase, thus increasing the pressure in that region. This pressure builds until it ultimately repels the incoming mass-energy and causes incoming baryons to rebound. The rebounding baryons form a pressure wave that propagates.

This is just what happens with sound (acoustic) waves, although the pressure there is due to gas molecules interacting with other gas molecules, not photons. With everyday sound waves, high and low density regions propagate due to the pressure variations between those regions. The speed of those waves for an ideal gas (which the plasma approximates) is

$$c_{sound} = k\sqrt{p / \rho} \tag{1}$$

where p is pressure, ρ is density, and k is an appropriate constant.

Thus, the baryon-photon plasma ends up with a whole spectrum (all different wavelengths) of essentially acoustic waves propagating through it in all directions.

Note that photons interact with electrons as well as baryons, but the mass of the electrons is so much smaller than that of the baryons that they are effectively "slaves" to the motion of the baryons and carried along with them. Their effect is insignificant, so they can be ignored.

2.2 Traveling Waves to Standing Waves

From elementary physics we know that two oppositely moving waves (along a string for example), will form a standing wave if they have the same wavelength. See Fig. 2.

Note that if traveling waves have different wavelengths, they will destructively interfere and not produce a standing wave. On average, waves of differing wavelengths will cancel one another out, but those of the same wavelength will tend to produce standing waves.

Over a given length (say of string between two walls) L, the standing waves formed must have lengths of $\lambda_n = 2L/n$, where $n = 1, 2, \ldots\infty$. The fundamental wave ($n = 1$) would have $\lambda = 2L$, i.e., it would have nodes at its ends (as in no motion where the string is pinned to the walls on either end) but none intermediate. (See the LH side of Fig. 3 below.) It would be half of a spatial sine wave oscillating up and down in time. The first harmonic ($n = 2$) would be a full sine wave with one node in the middle. Each higher harmonic would have one more node. Higher n means shorter wavelength and higher oscillating frequency in time ν, since $c_{sound} = \nu\lambda$.

two traveling waves
(same wavelength)

one standing wave
(different times shown)
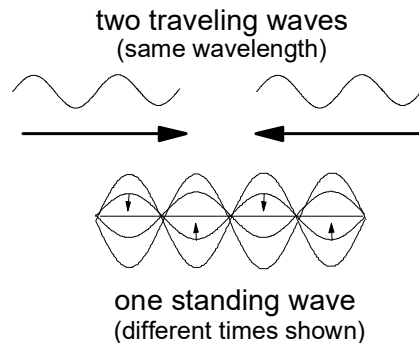
**Fig. 2 Standing Waves Forming from Traveling Ones**

The sound waves in the baryon-photon plasma interact with one another, destructively interfering in some regions and forming standing waves, via constructive interference, in others. These standing waves are referred to as <u>baryonic acoustic oscillations (BAOs)</u>.

2.3 Which Wavelengths Get Preferred (Form Standing Waves)

Standing waves in the universe (at the 380,000 year mark) can only form over lengths equal to the distance an acoustic wave could travel in 380,000 years. At greater distances, traveling waves (traveling at the speed of sound for the medium) would not have time to completely overlap and form a standing wave.

If we call the distance sound can travel in that 380,000 years L, then at that time, we would expect to find standing waves of wavelengths $\lambda_n = 2L/n$. Only those, in the time available since the creation event, would be able to neatly overlap in a constructive way. Other wavelength waves would randomly cancel one another through destructive interference.

We can think heuristically of $L = (c_{sound})(t_{recombin})$, where $t_{recombin}$ is 380,000 years in appropriate units, but note that due to pressure and density changes as the universe evolves, c_{sound} varies over time, so we would need to integrate to find L, rather than use a simple multiplication. Additionally, the universe continually expands, so any length L one might determine at one point in time gets stretched at later times. Cosmologists can readily make the appropriate calculations to get the distance L sound could travel from the first instant of creation up to the 380,000 year mark.
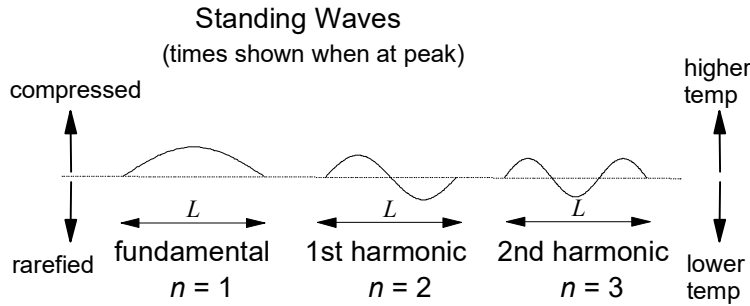

Figure 3. Fundamental Standing Wave and First Two Harmonics

All else being equal, the standing waves of wavelengths λ_n would be spread randomly at different amplitudes and in different directions.

2.4 Caveat on Wave Shape

To keep things simple and illustrate a point, we have depicted the acoustic wave shapes as sinusoids, but they are actually more complicated. Certainly, the usual sound waves with which we are familiar typically have more diverse shapes, though they can be analyzed as summations of sinusoids via Fourier series analysis. In fact, from both theory and analysis of the CMB, it is believed that via inflation, the large scale BAOs emerged, at least in large part, from primordial quantum harmonic oscillator fluctuations. Further, it appears the fundamental (lowest) state of those oscillators was, by far, the largest contributor to the fluctuations.

From elementary QM, we know (look it up if you don't recall) that the fundamental mode shape in space of a QM oscillator is Gaussian. See Fig. 4. The wave function ψ, and hence its probability density $|\psi|^2$, are normal (bell shape) curves in space. Thus, after inflation, the mass density would be expected to have similar shape.

$$\psi = \sqrt{\frac{1}{\sigma\sqrt{2\pi}}}\, e^{-\frac{x^2}{4\sigma^2}} \quad \rightarrow \quad |\psi|^2 = \frac{1}{\sigma\sqrt{2\pi}}\, e^{-\frac{x^2}{2\sigma^2}}$$
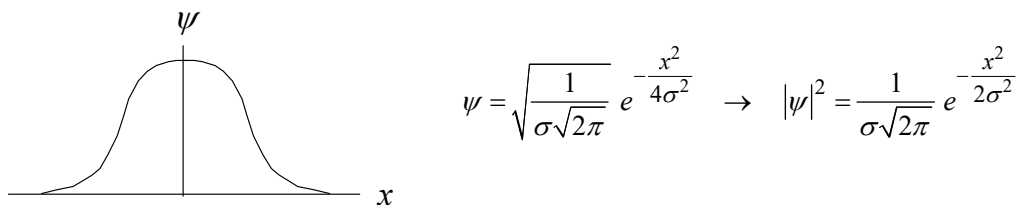
Figure 4. Gaussian Wave Form in Space for Ground State of Quantum Harmonic Oscillator

The growth of pressure (sound) waves from density fluctuations described in Sect. 2.1 would then, via the appropriate dynamics, lead to sound waves (BAOs) of similar, Gaussian shape. So, the $n = 1$ wave of Fig. 3 should be more Gaussian shaped than sinusoidal, though a Fourier analysis of it would have a large (half wave) sinusoidal component. Similarly, the peaks and valleys between nodes of the other modes (such as $n = 2$ and 3 of Fig. 3) would actually be quite close to Gaussian shape. But again, a Fourier analysis would have large components corresponding to the sinusoids shown in Fig. 3.

Even though the wave forms are more Gaussian than sinusoidal, we can still consider them to have modes of particular wavelengths (shorter for higher mode number n) with $n + 1$ nodes. We may, elsewhere in this document, depict the sound waves graphically as sinusoidal for simplicity, but keep the points of this section in mind as you contemplate that material.

2.5   Phases of the Various Acoustic Waves

Note that all the wave formation started at the same time. So, for example, all of the various fundamental modes (corresponding to $n = 1$ in Fig. 3) would have their corresponding traveling waves begin to propagate at the same time. They all propagate at the same speed and are subject to the same dynamics. So, the many different fundamental standing waves set up all over the universe would all be in phase in time and remain so as time progresses. Ditto for higher modes. Hence, all BAO standing waves throughout the universe having the same number of nodes remain in phase in time, i.e., all having the same mode number n peak at the same time.

2.6   Pressure (Acoustic) Waves to Photons of Various Frequencies (Temperatures)

Wherever the standing waves are denser, the pressure is higher. Higher pressure means hotter baryons (moving faster = higher energy). In interactions with photons, the baryons would impart more energy to the photons, resulting in higher frequency light emanating from the denser regions. Measuring the light frequency at a given point in space would then be equivalent to measuring temperature at that point.

In short, for a local region of baryons,

$$\text{higher } \rho \rightarrow \text{ higher } p \rightarrow \text{ higher } T \rightarrow \text{ higher frequency of } \gamma \text{ scattered.}$$

2.7   Freezing the Temperature (Photon Frequency) Patterns at 380,000 Years

At around 380,000 years after the big bang, average temperature of the universe had fallen to the point where baryons could capture electrons and form atoms (mostly protons and electrons to form hydrogen, but small amounts of helium and lithium atoms were also formed.) This point in time is, strangely enough, called <u>recombination</u>, even though it was the first time particles combined to form atoms, not a "recombining", which implies it had happened before. (And some think physics can be confusing....) [Added May 15, 2019 →] This naming is due to a historical misunderstanding of earlier epochs. A better name would be "decoupling".

Once recombination occurred, there was no longer a charged baryonic plasma scattering photons wildly and regularly. The atoms, with exceptions so rare as to not matter, did not scatter the photons, so the photons were effectively released from their electromagnetic bondage to baryonic matter. The photons streamed forth and spread outward through the rest of the universe.

The key point is that at that moment ("cosmic" moment), the photon frequencies reflected the temperatures of the local regions they last were in contact with. These frequencies were, in effect, "locked in" until the present day. Those variations in frequency are what COBE, WMAP, Planck, and other experiments have recently measured. That, including the average background temperature/frequency at 2.725° K, is the cosmic microwave background radiation (CMBR).

Note however, that due to the expansion of the universe since recombination, the frequencies of all photons have been reduced (wavelength stretched by expansion). This is taken into account when the photon frequencies data is analyzed. The relative differences remain as all photons are stretched by the same ratio by cosmic expansion (subject to some subtleties that we won't get into). [Added May 15, 2019 →] The universe has

expanded (in a linear direction) by a factor of 1100 since recombination. This means the average distance between CMBR photons, which was about 1 cm upon release, is now about 11 meters.

2.8 Phases of Different Modes at Recombination

As noted in Sect. 2.5, pg. 4, for a given mode number, the various individual local standing waves of that mode are all in phase in time (but scattered all over randomly in space at different amplitudes) and peak at the same time. However, the different modes oscillate at different frequencies, so waves of different mode numbers peak at different times. This is illustrated for the lowest three modes in Fig. 5.

Note that for fundamental ($n = 1$) mode oscillation frequency f_1, the nth mode has oscillation frequency equal to nf_1. So in the time it takes the $n = 1$ mode to oscillate ¼ of a full cycle, the $n = 2$ mode has oscillated through ½ of a full cycle. And the $n = 3$ mode has oscillated through ¾ of a full cycle.

Further, the fundamental standing wave at recombination (one hump as for $n = 1$ in Fig. 5) results from a local high density region acting as a gravitational attractor pulling in baryons. At recombination time, there has just been enough time to pull in baryons, but not enough time for pressure to have started them moving away from the center of the region. In other words, the $n = 1$ mode at recombination is a purely compressive hump. It is ¼ of the way through a full cycle (90° in phase). We will see that this results in the first peak shown in Fig. 1, pg. 1.
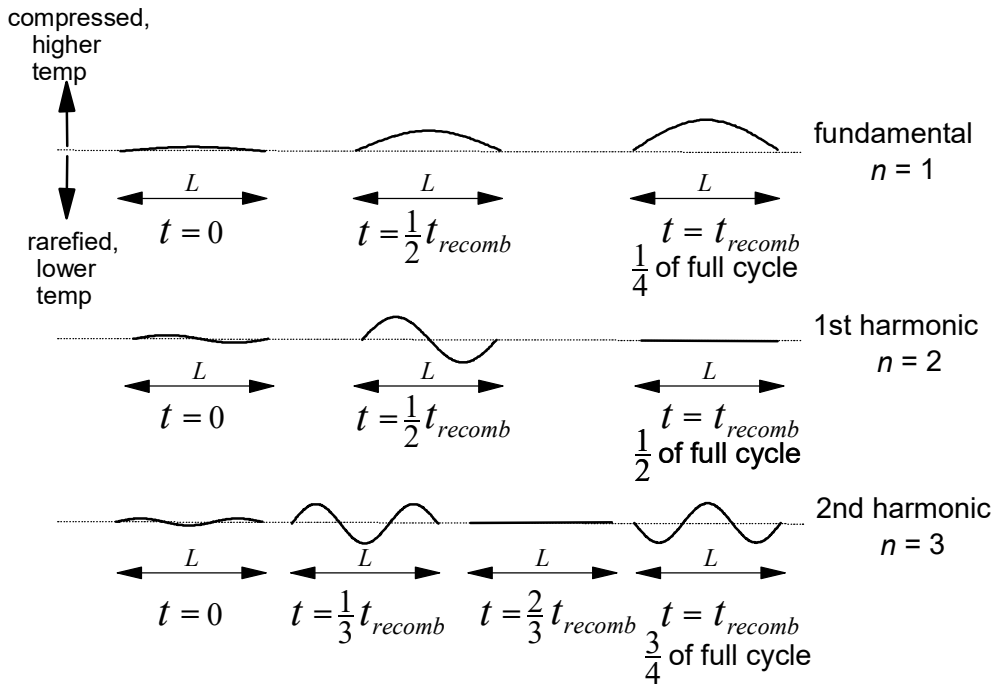
Figure 5. Evolution of the First Three Standing Wave Modes to Recombination Time

The $n = 2$ mode, on the other hand, with a compressive hump and a rarefied hump (three nodes), oscillates twice as fast as the $n = 1$ mode. So by the time of recombination, it has oscillated ½ of a full cycle (180° in phase). But that is simply a straight line. So we would not measure any real pressure/temperature increase in that region at that particular time. It would, effectively, not show up in our data. This results in the first trough after the first peak in Fig. 1.

The $n = 3$ mode, with four nodes, oscillates three times as fast as the $n = 1$ mode. So by the time of recombination, it has oscillated ¾ of a full cycle (270° in phase). This results in two rarefied humps and one compressive hump (an overall regional average of rarefied). This shows up as the second peak in Fig. 1.

Higher modes lead in similar fashion to subsequent troughs and peaks in Fig. 1.

2.9   The Last Scattering Surface

For us, as we look out into the universe, we look into the past, due to the great distances light must travel to reach us over the history of the universe. Looking in any direction, the light from recombination (CMB) reaches us from the same distance away, from all directions, at the same time. Thus, it is effectively coming, from our perspective, from a vast shell at a distance all but several hundred thousand light years from the edge of the visible universe. Hence, that shell looks to us like the surface of a giant sphere.

Since this spherical shell represents the last light to be scattered from primordial free baryons, it is call the last scattering surface (LSS).

The modes of Fig. 5, and higher modes, we see now are those from the LSS. But the LSS is best treated in a spherical coordinate system and we have been working with waves in a Cartesian system. The next two Sects. 3 and 4 show how we go from that Cartesian system to the spherical system in which our measurement of the CMB is carried out.

3   Plane Standing Waves in a Spherical Analysis

3.1   Graphically for Simplified Case

Consider one plane wave of the fundamental baryon acoustic mode (similar to $n = 1$ in Fig. 3). Pretend, for the sake of this discussion, that at the time of recombination, the wave extends in its direction of travel across the universe. That is, over each length L of Sect. 2.3, the fundamental standing wave is repeated. Things are actually far more diverse than this with various modes overlapping in various directions all over the place. However, we simplify here to make a point. We represent this simplification in Fig. 5.

Fig. 5 is almost self-explanatory. The fundamental wave of the figure is frozen after recombination. The baryons were most compressed at the peaks right before recombination, so photons that emanated from those regions are hottest (higher frequency). The nodal regions were not so compressed, and the photons from those are colder (lower frequency).
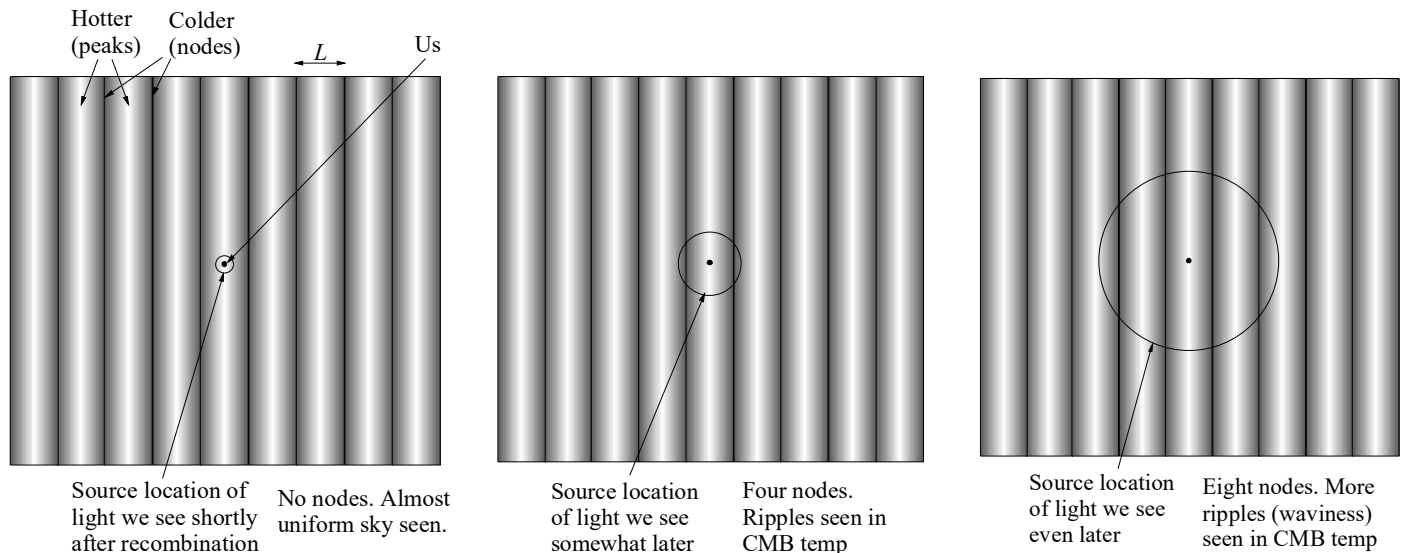
Figure 6. Over Time, Plane Waves Appear As Higher and Higher Modes on Sphere from which Light Reaching Us Left

Just after recombination (left most part of Fig. 6) light from the time of recombination had not traveled very far to reach us, so we can't yet see much variation in temperature of the photons reaching us. Somewhat later (middle part of Fig. 6), the light reaching us from that time is from further away, so we start to see some nodes.

At a later time, we would see more nodes, as in the right hand part of Fig. 5. As time goes on, we would see more and more nodes (higher modes) appearing on the spherical shell of the last scattering surface (LSS).

Note that if the middle figure were just a bit earlier, with the circle just touching the dark lines (nodal lines), we would see a quadrupole (2 colder regions and 2 hotter regions in 360º). Higher and higher *n*-poles appear as time goes on. At the present time, a fundamental standing wave from recombination of the ideal wave shown in Fig. 6 (which is not the case in nature) would appear to us to have hundreds of nodes, spaced a little less than one degree apart.

3.2 The Real, Not Ideal, Case

Of course, we don't have the ideal situation as in Fig. 6, where a single wave form repeats itself perfectly, over and over, across the universe. What we actually have are a whole slew of small waves of various lengths between humps (see Fig. 3) all over the place, depicted schematically in Fig. 7.

Only waves on last scattering surface shown. Others spread everywhere.

Symbolized as
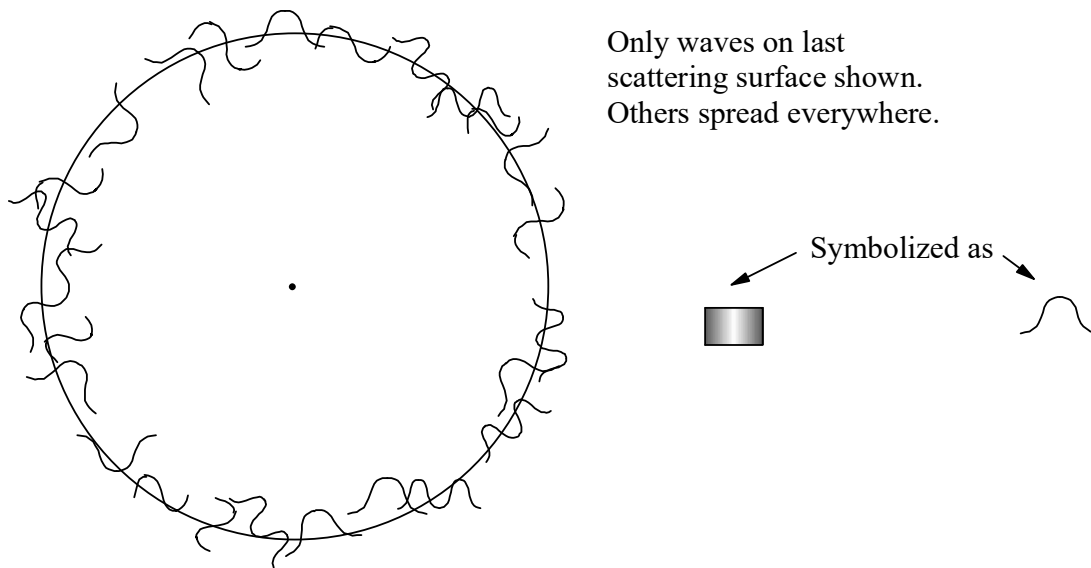
Figure 7. Some Local Gaussian Shaped Temperature Standing Waves on Last Scattering Surface (Only lower modes shown)

For a local fundamental wave (one hump, $n = 1$) the space between nodes at our present time would be a little less than one degree.

3.3 Converting Plane Waves to Spherical Coordinates

Because a plane wave, such as those of Figs. 5 and 6, appears to us as ripples on a spherical surface, our preferred method of analyzing data from those ripples is with a spherical coordinate system. To do that, one needs to convert a plane wave expressed in Cartesian coordinates (which is the easiest way to express a plane wave) into spherical coordinates. This is done via a mathematical relation known as Rayleigh's plane wave expansion, which we will present after discussing spherical harmonics in Sect. 4.

4 Spherical Harmonic Analysis

4.1 Background

Our data is a map of the temperature variations of the cosmic microwave background (CMB) radiation in the sky, and thus is taken effectively over a spherical shell. So, if we want to break down the temperature signal we see via a modal analysis, it is best to use the spherical analog of a Fourier spectral analysis, i.e., spherical

harmonic spectral analysis. The central concept behind spherical harmonic analysis is explained briefly in the following paragraphs, with a more in depth treatment in Appendix A.

A spherical harmonic series parallels the Fourier series, but we use spherical coordinates θ and ϕ. rather than Cartesian ones.

$$f(\theta,\phi)=\sum_{l=0}^{\infty}\sum_{m=-l}^{l}a_{lm}Y_{lm}(\theta,\phi) \qquad \left(\begin{array}{l} Y_{lm}(\theta,\phi) \text{ and } a_{lm} \text{ are generally complex, though they} \\ \text{can result in a real function } f(\theta,\phi), \text{ as in our case.} \end{array}\right) \qquad (2)$$

$$\text{similar to } f(x)=\sum_{n=0}^{\infty}A_n\left(\cos nkx+i\sin nkx\right)=\sum_{n=0}^{\infty}A_n e^{inkx}$$

$$\text{or in flat 2D, } f(x,y)=\sum_{n_x=0}^{\infty}\sum_{n_y=0}^{\infty}\underbrace{A_{n_x n_y}}_{\substack{\text{analogous} \\ \text{to } a_{lm}}}\underbrace{\left(\cos n_x kx+i\sin n_x kx\right)\left(\cos n_y ky+i\sin n_y ky\right)}_{\text{analogous to } Y_{lm}(\theta,\phi)}=\sum_{n_x=0}^{\infty}\sum_{n_y=0}^{\infty}A_{n_x n_y}e^{in_x kx}e^{in_y ky} \qquad (3)$$

Unfortunately, the spherical harmonics $Y_{lm}(\theta,\phi)$ are not of as simple a form as the sines and cosines of the linear dimension case. (See Appendix A for an extensive development of spherical harmonics.) However, just as the Fourier components (the harmonics, one for each n value in 1D) are orthogonal over a given spatial interval, the spherical harmonics $Y_{lm}(\theta,\phi)$ are mutually orthogonal on the surface of a sphere (over the intervals $0 < \theta < \pi$ and $0 < \phi < 2\pi$).

(2) is what is used in quantum mechanics for the hydrogen atom solution to the Schroedinger equation in spherical coordinates, so you have probably seen a relation like this before (with a complex wave function ψ, rather than a real f). Each a_{lm} represents the amplitude of a particular spherical harmonic component in the summation. In the hydrogen atom we were also concerned about the r direction and had a separate solution which was only a function of r (the Shroedinger equation was separable into a purely r dependent part and a part dependent on θ and ϕ. Here we ignore the r dependence since we are only concerned with describing a function [the temperature variations] of angular location, i.e., effectively on the surface of a sphere.)

The "l" index, an integer, is associated with the number of spatial oscillations (nodes, to be precise, equal to $l + 1$) in the θ direction in spherical coordinates, and "m", the number of spatial oscillations (nodes) in the ϕ direction. m, also an integer, varies from "$-l$" to "l" (recall the hydrogen atom). For example, the $l=0$ mode has zero oscillation in the θ direction, i.e., a monopole, or constant value over the whole sphere, that sets the overall scale. $l=1$ is a dipole: one full oscillation over the sphere in the θ direction. Go to higher and higher l values, and you get more spatial oscillations (and therefore smaller wavelength) over the sphere surface. The l and m integers of spherical coordinate analysis are analogous to the n_x and n_y integers of (3) for Cartesian coordinate analysis. The a_{lm} are analogous to the Fourier amplitudes $A_{n_x n_y}$.

4.2 Finding the a_{lm}

Note that since the Y_{lm} are orthonormal and complete over a sphere at fixed radius r (see Appendix A, Sect. 11.4 pg. 30) the a_{lm} can be determined (Sect. 11.5.1 pg.32, eq. (81)) as

$$a_{lm}=\int_0^{2\pi}\int_0^{\pi}Y_{lm}^*(\theta,\phi)f(\theta,\phi)\sin\theta\,d\theta\,d\phi. \qquad (4)$$

4.3 CMB Spherical Harmonics

Note with the CMB that we are dealing with a scalar function over the sphere surface, i.e., the temperature T. For us,

$$f(\theta,\phi)=T(\theta,\phi) \qquad (5)$$

The $l = 0$ component (zero spatial oscillation) spherical harmonic in (2) is $Y_{00} = 1$, so a_{00} would equal the mean temperature $\overline{\overline{T}} = 2.725^{\circ}\text{K}$, which is the constant background over the entire sky. The variation from the mean, ΔT, as a function of θ and ϕ, are analyzed in terms of its spherical harmonic components $Y_{lm}(\theta,\phi)$ for $l > 0$. Because T is a scalar, there are no issues of what direction our harmonic spatial waves are oscillating in. That is, we don't have to worry about longitudinal vs transverse directions for a scalar. Our temperature waves are scalar waves, so variations are merely numbers.

4.4 Expressing Plane Standing Waves in Spherical Coordinates

4.4.1 A Simple Complex Sinusoid

The relation alluded to in Sect. 3.2 for expressing a plane standing wave in spherical coordinates is known as Rayleigh's plane wave expansion. (See http://en.wikipedia.org/wiki/Plane_wave_expansion.) We state it here without proof as (6). For a single (complex) sinusoidal wave of unit amplitude with wave vector $\mathbf{k}$ (having wave number k pointing along unit vector $\mathbf{n_k}$), where $\mathbf{r}$ is the vector from the origin to the point in question (having length r pointing along unit vector $\mathbf{n}$), where $\theta_{\mathbf{k}}$, $\phi_{\mathbf{k}}$ and θ, ϕ are the spherical coordinate angles for $\mathbf{n_k}$ and $\mathbf{n}$, respectively, and where $j_l(kr)$ are spherical Bessel functions,

$$\underbrace{e^{i\mathbf{k}\cdot\mathbf{r}}}_{\substack{\text{coordinate} \\ \text{independent} \\ \text{form}}} = \underbrace{e^{ik_x x}e^{ik_y y}e^{ik_z z}}_{\substack{\text{Cartesian} \\ \text{coordinates}}} = \underbrace{4\pi\sum_{l=0}^{\infty}\sum_{m=-l}^{l} i^l j_l(kr)Y_{lm}^*(\theta_{\mathbf{k}},\phi_{\mathbf{k}})Y_{lm}(\theta,\phi)}_{\text{spherical coordinates = Rayleigh expansion}} \tag{6}$$

4.4.2 Arbitrary Plane Wave Shapes

Any wave shape other than a sinusoid, such as a sum of local Gaussian waves over the whole sky (Fig. 7. pg. 7), can be expressed, in the spirit of Fourier harmonic analysis, in Cartesian coordinates (bounded by a box L_x by L_y by L_z in the discrete solution case) as

$$\underbrace{f(\mathbf{r})}_{\substack{\text{arbitrary} \\ \text{wave form}}} = \underbrace{f(x,y,z)}_{\substack{\text{Cartesian} \\ \text{coordinates}}} \quad \left(\begin{array}{l} f(\mathbf{r}) \text{ could be temperature pattern at all } \mathbf{r} \text{ in all of space at the present time of} \\ \text{photons scattered at recombination, i.e., a sum of all Gaussian local temperature variations} \end{array} \right)$$

$$\text{for discrete case} = \sum_{n_x=-\infty}^{\infty}\sum_{n_y=-\infty}^{\infty}\sum_{n_z=-\infty}^{\infty} A_{n_x n_y n_z} \underbrace{e^{in_x k_{1x} x}e^{in_y k_{1y} y}e^{in_z k_{1z} z}}_{\substack{\text{complex sinusoids,} \\ \text{Cartesian coordinates}}} \quad k_{1x} = \frac{\pi}{L_x} \quad k_{1y} = \frac{\pi}{L_y} \quad k_{1z} = \frac{\pi}{L_z} \tag{7}$$

$$\text{for continuous case} \qquad = \frac{1}{(2\pi)^3}\int A(\mathbf{k})\overbrace{e^{ik_x x}e^{ik_y y}e^{ik_z z}}\,d^3k = \frac{1}{(2\pi)^3}\int A(\mathbf{k})e^{i\mathbf{k}\cdot\mathbf{r}}\,d^3k.$$

The same wave shape can be expressed, in the spirit of spherical harmonic analysis, as

$$\underbrace{f(r,\theta,\phi)}_{\substack{\text{same wave} \\ \text{form, spher} \\ \text{coords}}} = \sum_{l=0}^{\infty}\sum_{m=-l}^{l} a_{lm} j_l(kr)Y_{lm}(\theta,\phi) \tag{8}$$

By using (6) in (7) and equating the result to the RHS of (8), one can obtain relationships between the a_{lm} coefficients of spherical harmonic analysis and the $A_{n_x n_y n_z}$ (or $A(\mathbf{k})$) of Cartesian harmonic analysis. We will keep things simple at this point and hold off until Sect. 7.4 to do this. For now, we simply note the implications of doing so.

Bottom line: If we have a theory developed for standing wave formation in Fourier components in Cartesian coordinates, we can deduce the a_{lm} we would expect to measure for that formation in a spherical coordinate

system. Conversely, if we have data, i.e., the a_{lm}, taken in a spherical coordinate system, we can determine the corresponding Fourier components $A_{n_x n_y n_z}$ (or $A(\mathbf{k})$) for theoretical analysis. This is done in analyzing the CMB.

5   The CMB and the Amplitude a_{lm} of Each Spherical Harmonic Y_{lm}

5.1   Measuring for the CMB

The spherical harmonics Y_{lm}, individually, are not pure sines or cosines, though they are oscillating spatial wave forms. (See Appendix A, pg. 29, eq. (65) for the θ dependence of several of the lowest modes.) Showing them graphically in what follows would not be easy, so we won't do that. However, the a_{lm} amplitudes of (2) and (4) are analogous to amplitudes of sine waves.

5.2   Measuring the CMB Amplitude and Variance

5.2.1   Measurement in Our Universe

Recall the CMB radiation displays the acoustic standing wave patterns that existed right at recombination. In other words, we have a cosmic snapshot at one time (recombination), and for any given mode (such as the fundamental with $n = 1$), all localized plane waves everywhere would be in phase. (See Fig. 5, pg. 5.) But the heights of the individual standing waves of the same mode would vary from individual wave to individual wave.

As shown in Sect. 4.4.2, pg. 9, the sum of many plane waves of many modes at many different locations can be converted to spherical harmonic representation with a given amplitude coefficient a_{lm} associated with each Y_{lm}. Thus, the particular a_{lm} we measure would be those at the time of recombination in our universe. In other universes with the same laws but different initial conditions (different set of random density fluctuations), at their recombination times, we would have different a_{lm}.

5.2.2   Measurement Over an Ensemble of Universes

Consider having an ensemble of universes we could collect data from. Each is structured in the same manner as ours, with the same physicals laws, particles, and parameters (same curvature, baryon density, dark matter, dark energy, photon density, etc.) However, each has different initial conditions, i.e., random QM fluctuations at the onset of inflation, and these occur randomly throughout members of the ensemble.

If we did have a lot of universes similar to ours and could make many measurements (one in each such universe), a given a_{lm} would vary in value between them. It would be positive in approximately half of them and negative in half, with the average a_{lm} over all universes tending to zero as the number of universes got large. Since our mean value for a_{lm} ($l > 0$) would tend to zero, it is not of great use to us as a characterizing parameter of the CMB.

The variance (or, equivalently its square root, the standard deviation) of a_{lm} ($l > 0$), however, is related to the squares of the a_{lm} and thus must be a positive number, and not tend to zero. It would give us a measure of how great a contribution a particular spherical mode (given l and m) makes to the physics of universes like ours. If we could somehow get an experimental value for that variance of a_{lm} over an ensemble of universes, we would, as the saying goes, "be in business".

There actually is a trick that does something close to this, and we discuss it in the next section.

5.2.3 A Trick to Get Many Measurements from Our One Universe

We don't have any extra universes similar to ours we can access to make extra measurements of a_{lm} in each, so what do we do?

If we consider that for given l, each m is equally likely to have the same measured a_{lm} value, then measuring those m modes effectively gives us what we would get from extra measurements in different universes. If we average a_{lm} ($l > 0$) over all m for a given l, we will tend to get zero, just as we noted in Sect. 5.2.2 for an average over different universes. So, mean value for a_{lm} ($l > 0$) over all m isn't of much use to us.

However, if we average the square of a_{lm} over all m for a given l we will tend to get a non-zero value, such as we noted in Sect. 5.2.2 for different measurements in different universes. Since $-l < m < l$, we have $2l + 1$ values of m to use. For fairly large l, this essentially means good statistical values approaching the true values to high confidence.

Thus, we want to compute, for each l value, the variance, which is labeled C_l, as

$$\boxed{\overline{|a_{lm}|^2} = \left\langle |a_{lm}|^2 \right\rangle = \left\langle a_{lm}^* a_{lm} \right\rangle = \frac{1}{2l+1} \sum_{m=-l}^{+l} a_{lm}^* a_{lm} = C_l \qquad \text{no sum on } l}$$

(9)

where the average symbol $\langle \ \rangle$ is considered to be for all m values (given a single l value) in our universe now.

Caution that in the literature, C_l is sometimes taken as the average over all m values as above, and sometimes as just the value for a single m, as below.

Sometimes one sees $\qquad \left\langle a_{l'm'}^* a_{lm} \right\rangle = a_{l'm'}^* a_{lm} \, \delta_{l'l} \delta_{m'm} = C_l$

(10)

where the average symbol $\langle \ \rangle$ is considered to be for a single m value (and single l value) over many universes.

The connection between the two versions lies in the presumption that (10) for given l, over a large number of universes, would be the same for any m (each m mode would tend to have the same power). Thus, the average over all m, for given l, as in (9), would tend to equal (10). (10) is theoretical (we can never measure other universes), but (9) is something we can measure experimentally with the CMB data. We can, in fact, get $2l + 1$ separate measurements, implying, for large l, considerable confidence the computed value (9) is an accurate reflection of what is really going on (and not a statistical aberration.)

Since power of any wave is proportional to the square of the amplitude of that wave, the variance can be thought of as a measurement of the power of the l mode (including all m values for that l for (9)). Plotting C_l vs l is called a power spectral analysis. (See Appendix B for an introduction to [review of] the theory of power spectral analysis.) Subject to some further considerations to be discussed below, for the CMB, this gives us the power spectral analysis of Fig. 1 that has become so famous.

Note, in passing, that a system displaying the same statistics over many measurements in time or space as it does over many measurements from different similar systems in an ensemble is called <u>ergodic</u>. Here we are averaging over different measurements in space (spherical coordinate space) with the presumption that gives us the same statistical results as measuring over different universes. So our system is an ergodic one.

5.3 The Key Relationship

Note that if we use (4) with $f(\theta, \phi) = T(\theta, \phi)$ in (9), we get

$$C_l = \left\langle |a_{lm}|^2 \right\rangle = \left\langle a_{l'm'}^* a_{lm} \right\rangle = \frac{1}{2l+1} \sum_{m=-l}^{+l} a_{l'm'}^* a_{lm} \qquad \text{no sum on } l$$

$$= \frac{1}{2l+1} \sum_{m=-l}^{+l} \left(\int_0^{2\pi} \int_0^{\pi} Y_{lm}(\theta',\phi') T(\theta',\phi') \sin\theta' \, d\theta' \, d\phi' \right) \left(\int_0^{2\pi} \int_0^{\pi} Y_{lm}^*(\theta,\phi) T(\theta,\phi) \sin\theta \, d\theta \, d\phi \right) \quad (11)$$

$$= \frac{1}{2l+1} \underbrace{\int_0^{2\pi} \int_0^{\pi}}_{\int_{\Omega}} \underbrace{\int_0^{2\pi} \int_0^{\pi}}_{\int_{\Omega'}} \left(\sum_{m=-l}^{+l} Y_{lm}(\theta',\phi') Y_{lm}^*(\theta,\phi) \right) T(\theta',\phi') T(\theta,\phi) \underbrace{\sin\theta' d\theta' \, d\phi'}_{d\Omega'} \underbrace{\sin\theta d\theta \, d\phi}_{d\Omega}.$$

To streamline notation, we can use unit vector notation, where **n** is the unit vector pointing in the θ, ϕ direction and **n′** is the unit vector pointing in the θ', ϕ direction. Thus, (11) is re-written as

$$\boxed{\begin{aligned} C_l &= \frac{1}{2l+1} \int_{\Omega} \int_{\Omega'} \left(\sum_{m=-l}^{+l} Y_{lm}(\theta',\phi') Y_{lm}^*(\theta,\phi) \right) T(\theta',\phi') T(\theta,\phi) \, d\Omega' d\Omega \\ &= \frac{1}{2l+1} \int_{\Omega} \int_{\Omega'} \left(\sum_{m=-l}^{+l} Y_{lm}(\mathbf{n}') Y_{lm}^*(\mathbf{n}) \right) T(\mathbf{n}') T(\mathbf{n}) \, d\Omega' d\Omega. \end{aligned}} \qquad (12)$$

5.4 Finding C_l Experimentally

We have a data set of discrete points of the CMB where each point has a T value and an associated θ, ϕ (or equivalently an **n**). That is, we have $T(\theta,\phi) = T(\mathbf{n})$ in digital format. We can process this data via computer in either of two equivalent ways. The second is simpler and is preferred.

First way

Step 1. Use $f(\theta,\phi) = T(\theta,\phi) = T(\mathbf{n})$ in (4) to determine a_{lm}.

Step 2. Use a_{lm} in (9).

Second way

An equivalent, and one step way, is simply to use (12) (which is simplified below in (14)).

5.5 Things to Know about C_l

5.5.1 Nomenclature and Units

C_l is the <u>variance</u> of the spherical harmonic amplitudes a_{lm} for fixed l. It is also known as the <u>l component of</u> the <u>power spectrum</u> of the CMB (square of wave amplitude is proportional to power in a wave). Further, in its dependence on l, it is known as a <u>correlation function</u>, for reasons discussed in Sect. 5.5.2.

If $f(\theta,\phi) = T(\theta,\phi)$ in (4) and the spherical harmonics Y_{lm} are unitless (which they are), then the a_{lm} have units of temperature. Hence, C_l, via (9), has units of $(\text{temp})^2$.

5.5.2 C_l as a Correlation Function

Consider (12), where for two different locations on the sphere of the CMB (directions we see in space) **n′** and **n**, the values of T are particularly high, i.e., local maxima. There exists a certain Y_{lm} at a given l which also has peaks (local maxima) at these locations. Thus, in the integral of (12) this particular contribution, from the T values at the two points, and the Y_{lm} values at those points, will make a larger contribution to the value of C_l than if the same pair of points did not display local maxima.

Thus we will get larger values of C_l for a given l if there are peaks in the sky correlated with the peaks we find in Y_{lm} for that l. Thus, we say C_l represents a correlation between points a certain distance apart in the

CMB. Actually it is a measure of the correlation between all points integrated over the whole sphere for given l. The more such points peak at the between peaks distance of the l spherical harmonic, the greater C_l. Thus, as a function of l, C_l is a correlation function.

5.5.3 Independence of C_l from Choice of Coordinate Reference Frame

One might question, from (12), if we would get different C_l for different choices for our coordinate axes. (See Fig. A-2, pg. 27). For example, for a different alignment of our z axis, the values for θ and ϕ would change for the two different points we integrate over, so one might expect the total integral to be different. However, the C_l actually are independent of choice of coordinate axes, as shown below.

Showing C_l independence from coordinate axes chosen

We will need something called the addition theorem for spherical harmonics, stated without proof below in (13). Note that P_l is the Legendre polynomial of order l. (See Appendix A Sect. 11.1, pg. 24.)

$$P_l \underbrace{\left(\mathbf{n}' \cdot \mathbf{n}\right)}_{\cos\theta_{\mathbf{n}'\mathbf{n}}} = \frac{4\pi}{2l+1} \sum_{m=-l}^{+l} Y_{lm}\left(\theta', \phi'\right) Y_{lm}^{*}\left(\theta, \phi\right) = \frac{4\pi}{2l+1} \sum_{m=-l}^{+l} Y_{lm}\left(\mathbf{n}'\right) Y_{lm}^{*}\left(\mathbf{n}\right) \tag{13}$$

$\theta_{\mathbf{n}'\mathbf{n}}$ is the angle between $\mathbf{n}'$ (aligned with θ', ϕ') and $\mathbf{n}$ (aligned with θ, ϕ). Using (13) in (12), we have

$$\boxed{C_l = \frac{1}{4\pi} \int_\Omega \int_{\Omega'} P_l\left(\mathbf{n}' \cdot \mathbf{n}\right) T\left(\mathbf{n}'\right) T\left(\mathbf{n}\right) d\Omega' d\Omega} \;. \tag{14}$$

Relation (14) only depends on the angle between two points in the sky and the temperature at each of those points. Hence, it is independent of the particular coordinate axes alignment chosen.

Also, (14) seems simpler to evaluate than (12), so my guess (not being a practitioner in the field) would be that it is the preferred way to analyze the data. That is, use (14) instead of (12) in Sect. 5.4.

An Example: The Dipole ($l = 1$)

One can best follow the following example by first becoming familiar with Appendix A, Sect. 11.5.5 pg. 35. Fig. A-3 there shows one of the simplest spherical harmonics, the one for $l = 1$, i.e., the dipole. In the figure, three different dipole alignments along with their particular spherical harmonic coefficients a_{lm} (for different m) are shown in the same coordinate system. However, an equivalent way to look at the figure is to consider the dipole fixed relative to the sky, but with different coordinate systems in each case. The a_{lm} for each coordinate system (for the same dipole) are different (and are shown in the referenced section). However, in the sum of (9) over m, we should get the same C_l in each case. The respective $|a_{lm}|^2$ contributions for each coordinate system in Fig. A-3 are shown summed together in the following chart.

Comparison Chart for Fig. A-3, pg. 36

$(l = 1 \rightarrow 1/(2l + 1) = 1/3$ in (9))

<u>Fig. A-3 a)</u>	<u>Fig. A-3 b)</u>	<u>Fig. A-3 c)</u>
$\frac{1}{3}\left(\lvert a_{1-1}\rvert^2 + \lvert a_{10}\rvert^2 + \lvert a_{11}\rvert^2\right) = C_l$	$\frac{1}{3}\left(\lvert a_{1-1}\rvert^2 + \lvert a_{10}\rvert^2 + \lvert a_{11}\rvert^2\right) = C_l$	$\frac{1}{3}\left(\lvert a_{1-1}\rvert^2 + \lvert a_{10}\rvert^2 + \lvert a_{11}\rvert^2\right) = C_l$
$\frac{1}{3}\left(0 + \frac{2X^2}{3} + 0\right) = \frac{2X^2}{9}$	$\frac{1}{3}\left(\frac{X^2}{3} + 0 + \frac{X^2}{3}\right) = \frac{2X^2}{9}$	$\frac{1}{3}\left(\frac{2X^2}{6} + \frac{X^2}{6} + \frac{X^2}{6}\right) = \frac{2}{9}X^2$

The conclusion: The C_l for the same pattern in the sky is the same as found in any coordinate system.

5.5.4 Local Variation Implications for C_l as a Correlation Function

We could consider either (12) or (14) and what happens for local maxima or minima temperature variations, though for simplicity, we will focus on (14). Fig. 8 depicts two local maxima schematically, projecting 3D to 2D for simplicity.
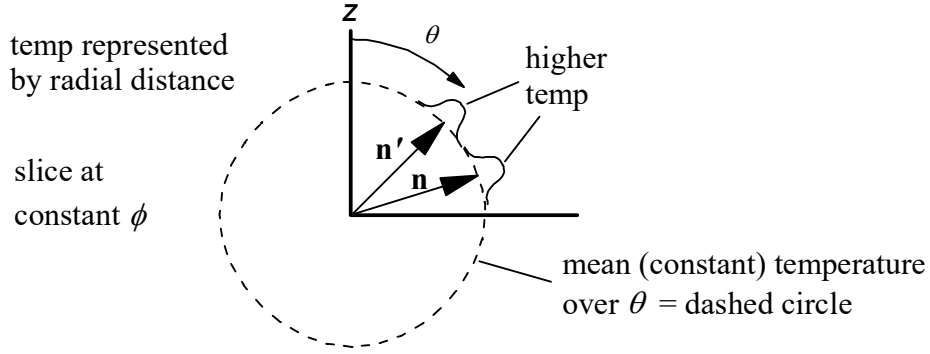
Figure 8. Two (Hypothetical) Local Maxima in CMB

In Fig. 8, we have two local solid angle regions where the temperature is higher than surrounding regions. That is, over a region of the integration of (14) (or (12)

$$T(\mathbf{n}')\Delta\Omega' \quad \text{and} \quad T(\mathbf{n})\Delta\Omega \qquad \text{both large for } \mathbf{n} \text{ and } \mathbf{n}' \text{ aligned as in figure .} \tag{15}$$

There is some Legendre polynomial $P_{l'}$, for some l', that peaks regularly at the angular distance between $\mathbf{n}$ and $\mathbf{n}'$. Thus, in the region of higher temperatures, we would get a greater contribution to the integral (14) from $P_{l'}$ than from other P_l.

$$P_{l'}(\mathbf{n}'\cdot\mathbf{n})T(\mathbf{n}')T(\mathbf{n})\Delta\Omega'\Delta\Omega \quad \text{high for regions where } \mathbf{n} \text{ and } \mathbf{n}' \text{ at temp peaks .} \tag{16}$$

For other regions, $P_{l'}$ may or may not peak, but the variation in T does not, so the other regions would not contribute so much to the integral (14) for $l = l'$.

$$P_{l'}(\mathbf{n}'\cdot\mathbf{n})T(\mathbf{n}')T(\mathbf{n})\Delta\Omega'\Delta\Omega \quad \text{low for regions where } \mathbf{n} \text{ and } \mathbf{n}' \text{ not at temp peaks} \tag{17}$$

For other l, and thus other P_l, the peaks in the P_l would not correspond to the peak temperature regions in Fig. 8, so we would not get as great a contribution.

$$P_l(\mathbf{n}'\cdot\mathbf{n})T(\mathbf{n}')T(\mathbf{n})\Delta\Omega'\Delta\Omega \quad \text{low for } l \neq l' \text{ even in regions where } \mathbf{n} \text{ and } \mathbf{n}' \text{ at temp peaks} \tag{18}$$

Note also that for l', if there were more regions of local maxima in other parts of the sky separated by the same angle as for those maxima in Fig. 8, we would have more contributions like that of (16) to (14) and a higher value for $C_{l'}$.

Bottom line: For given l, C_l is greater if there are more local extrema in the sky with angular separation of that displayed by the extrema in P_l. Thus, C_l provides a measure of the correlation between number and level of variations in CMB temperature the sky for a particular value of l.

Since l is inversely related to angular separation (angle = 180º/l), C_l is also represents a correlation between local extrema and their prevalence at a given angular separation.

5.6 The Variance of the Variance C_l

Note that C_l is measured only for our universe, so it will have some error in it even for large, but finite, l (where we have many m to sample and sum over in (9) or (12)). Of course, we expect the error to be less, the larger the l, since there are more samples taken (more m). But there is some error nonetheless. If we had a nearly infinite number of universes in an ensemble, we could make a nearly infinite number of measurements, and pin C_l down precisely. We are limited, instead, to our $2l + 1$ measurements for given l in the one universe we do have.

We express our unknown error in C_l as a confidence level, based on the usual relation for experimental standard deviation (19). (It is also common to use $N - 1$ in the denominator of (19), but cosmologists seem to use N.)

$$\text{Standard Deviation of } x = \sigma_x = \sqrt{\frac{\sum\limits_{i=1}^{N}(x_i - \bar{x})^2}{N}} \qquad N \text{ measurements .} \qquad (19)$$

For us, $\bar{x} = C_l$, our average over all m values ($2l + 1$ in number), as in (9). We have $N = 2l + 1$ measurements. So (19) becomes

$$\underbrace{\text{Standard Deviation of } |a_{lm}|^2}_{\text{Define as } \Delta C_l} = \sqrt{\frac{\sum\limits_{m=-l}^{+l}\left(|a_{lm}|^2 - C_l\right)^2}{2l+1}} \qquad \text{no sum on } l . \qquad (20)$$

So,

$$\frac{\Delta C_l}{C_l} = \sqrt{\frac{\sum\limits_{m=-l}^{+l}\left(\frac{|a_{lm}|^2}{C_l} - 1\right)^2}{2l+1}} \qquad \text{no sum on } l \qquad (21)$$

For some reason I have not been able to uncover, cosmologists assume the summation in the numerator of (21) is approximately 2. Thus,

$$\frac{\Delta C_l}{C_l} \approx \sqrt{\frac{2}{2l+1}} \quad \text{Cosmic variance} \quad (\text{no sum on } l) \quad \rightarrow \quad \text{standard deviation } \Delta C_l \approx \sqrt{\frac{2}{2l+1}}\, C_l . \quad (22)$$

Strangely, though the LHS of (22) represents a standard deviation (divided by C_l), it is called the <u>cosmic variance</u> (one more source for confusion on this issue, as variance is typically the square of the standard deviation). For one standard deviation at given l (= ΔC_l), our <u>confidence level</u> is 68%; for two, 95%. These are the error bars one sees in a typical plot of the C_l vs l. Note they are much wider for low l, than for higher values.

Keep in mind the difference between the "variance of the a_{lm}", which is C_l, and the "cosmic variance" ΔC_l which is the standard deviation of C_l (divided by C_l). ΔC_l is a "variance" (not really) of a variance (C_l).

6 Converting Between Cartesian Fourier and Spherical Harmonics Analyses

6.1 Express a_{lm} in Terms of Fourier Amplitude $A(\mathbf{k})$

As foreshadowed in Sect. 3.3, we will now express the spherical harmonic coefficients a_{lm} for a given CMB temperature distribution in terms of the Fourier component coefficients for the same distribution. We do this for the general case where a_{lm} can be at any radius r from the origin, not just at the radius of the LSS.

We start by repeating (4) for any sphere of radius r, with some alternate notation employing the unit vector $\mathbf{n}$ from the origin to the unit radius sphere, and with the arbitrary function f replaced with CMB temperature T.

$$a_{lm} = \int_0^{2\pi} \int_0^{\pi} Y_{lm}^*(\theta,\phi) \underbrace{T(\theta,\phi)}_{\text{at radius } r} \sin\theta\, d\theta\, d\phi = \int Y_{lm}^*(\mathbf{n}) T(\mathbf{r}) d\Omega \qquad \mathbf{r} = r\mathbf{n}. \qquad (4)$$

We then use the lowest row of (7), repeated below, which describes the CMB temperature everywhere (not just on the spherical surface of the LLS).

$$T(\mathbf{r}) = \frac{1}{(2\pi)^3} \int A(\mathbf{k}) \overbrace{e^{ik_x x} e^{ik_y y} e^{ik_z z}}^{\text{Cartesian form}} d^3 k = \frac{1}{(2\pi)^3} \int A(\mathbf{k}) \overbrace{e^{i\mathbf{k}\cdot\mathbf{r}}}^{\substack{\text{general} \\ \text{form}}} d^3 k . \qquad (7)$$

Now use the Rayleigh plane wave expansion (6)

$$e^{i\mathbf{k}\cdot\mathbf{r}} = 4\pi \sum_{l'=0}^{\infty} \sum_{m'=-l'}^{l'} i^{l'} j_{l'}(kr) Y_{l'm'}^*(\theta_{\mathbf{k}},\phi_{\mathbf{k}}) Y_{l'm'}(\theta,\phi) = 4\pi \sum_{l'=0}^{\infty} \sum_{m'=-l'}^{l'} i^{l'} j_{l'}(kr) Y_{l'm'}^*(\mathbf{n}_{\mathbf{k}}) Y_{l'm'}(\mathbf{n}) \qquad \mathbf{k} = k\mathbf{n}_{\mathbf{k}} \quad (6)$$

to express (7) in terms of spherical harmonics/coordinates.

$$T(\mathbf{r}) = T(r\mathbf{n}) = \frac{1}{(2\pi)^3} \int A(\mathbf{k}) \left(4\pi \sum_{l'=0}^{\infty} \sum_{m'=-l'}^{l'} i^{l'} j_{l'}(kr) Y_{l'm'}^*(\mathbf{n}_{\mathbf{k}}) Y_{l'm'}(\mathbf{n}) \right) d^3 k . \qquad (23)$$

Now put (23) into (4), where we use (78) of Appendix A in the second line,

$$a_{lm} = \int Y_{lm}^*(\mathbf{n}) \left(\frac{1}{(2\pi)^3} \int A(\mathbf{k}) \left(4\pi \sum_{l'=0}^{\infty} \sum_{m'=-l'}^{l'} i^{l'} j_{l'}(kr) Y_{l'm'}^*(\mathbf{n}_{\mathbf{k}}) Y_{l'm'}(\mathbf{n}) \right) d^3 k \right) d\Omega$$

$$= \frac{4\pi}{(2\pi)^3} \sum_{l'=0}^{\infty} \sum_{m'=-l'}^{l'} \left(\int A(\mathbf{k}) i^{l'} j_{l'}(kr) Y_{l'm'}^*(\mathbf{n}_{\mathbf{k}}) \left(\underbrace{\int \left(Y_{lm}^*(\mathbf{n}) Y_{l'm'}(\mathbf{n}) \right) d\Omega}_{\delta_{ll'} \delta_{mm'}} \right) d^3 k \right) \qquad (24)$$

$$= \frac{4\pi}{(2\pi)^3} \int A(\mathbf{k}) i^l j_l(kr) Y_{lm}^*(\mathbf{n}_{\mathbf{k}}) d^3 k, \qquad \begin{array}{l} \text{where } a_{lm} \text{ here is at radius } r \text{ from the origin,} \\ A(\mathbf{k}) \text{ is Fourier coefficient for } \mathbf{k} \text{ wave.} \end{array}$$

6.2 Express $C_l = \langle a_{l'm'}^* a_{lm} \rangle$ in Terms of Fourier Amplitudes $A(\mathbf{k})$

Now we will express the variance C_l in terms of $A(\mathbf{k})$ instead of $T(\mathbf{n})$ (as we did in (12) and (14)), and do so for any radius r.

First, we start with (9) or (10) (each uses a different way to take the mean), repeated below,

$$C_l = \langle |a_{lm}|^2 \rangle = \langle a_{l'm'}^* a_{lm} \rangle \qquad \text{no sum on } l, \qquad (9) \text{ or } (10)$$

and insert the last row of (24) into it twice.

$$C_l = \left\langle a_{l'm'}^* a_{lm} \right\rangle = \left\langle \left(\frac{4\pi}{(2\pi)^3} \int A^*(\mathbf{k}')(-i)^{l'} j_{l'}(k'r) Y_{l'm'}(\mathbf{n}_{\mathbf{k}'}) d^3 k' \right) \left(\frac{4\pi}{(2\pi)^3} \int A(\mathbf{k}) i^l j_l(kr) Y_{lm}^*(\mathbf{n}_{\mathbf{k}}) d^3 k \right) \right\rangle$$

$$= \frac{(4\pi)^2}{(2\pi)^6}(-i)^{l'} i^l \left\langle \int\int A^*(\mathbf{k}') A(\mathbf{k}) j_{l'}(k'r) j_l(kr) Y_{l'm'}(\mathbf{n}_{\mathbf{k}'}) Y_{lm}^*(\mathbf{n}_{\mathbf{k}}) d^3 k' d^3 k \right\rangle \qquad (25)$$

$$= \frac{1}{4\pi^4}(-i)^{l'} i^l \int\int \left\langle A^*(\mathbf{k}') A(\mathbf{k}) \right\rangle j_{l'}(k'r) j_l(kr) Y_{l'm'}(\mathbf{n}_{\mathbf{k}'}) Y_{lm}^*(\mathbf{n}_{\mathbf{k}}) d^3 k' d^3 k .$$

Second, we want to eliminate the primed quantities and simplify. To do this, we note in the last line of (25) that

$$\left\langle A^*(\mathbf{k}') A(\mathbf{k}) \right\rangle \rightarrow 0 \quad \text{for } \mathbf{k}' \neq \mathbf{k} , \qquad (26)$$

since $A(\mathbf{k})$ can be positive or negative, and in sums over many universes (or many times or many m), its value and its negative will at times pair with the same $A^*(\mathbf{k}')$ and those two terms will cancel. Over large sums, enough pairings arise to give a total value approaching zero as the number of universes (number of times, number of m values) approaches infinity.

However,

$$\left\langle A^*(\mathbf{k}') A(\mathbf{k}) \right\rangle \rightarrow (\text{some factor}) \left\langle |A(\mathbf{k})|^2 \right\rangle \neq 0 \quad \text{for } \mathbf{k}' = \mathbf{k} , \qquad (27)$$

where $\left\langle |A(\mathbf{k})|^2 \right\rangle$ is a variance in $\mathbf{k}$ space, similar in some ways to C_l in spherical harmonic space. This is some justification for the following, which is proven in Abramo and Pereira[1],

$$\left\langle A^*(\mathbf{k}') A(\mathbf{k}) \right\rangle = \left\langle |A(\mathbf{k})|^2 \right\rangle (2\pi)^3 \delta(\mathbf{k}' - \mathbf{k}) . \qquad (28)$$

With (28), the last line of (25) turns into

$$C_l = \frac{2}{\pi}(-i)^{l'} i^l \int \left\langle |A(\mathbf{k})|^2 \right\rangle j_l(kr) j_{l'}(kr) Y_{l'm'}(\mathbf{n}_{\mathbf{k}}) Y_{lm}^*(\mathbf{n}_{\mathbf{k}}) d^3 k . \qquad (29)$$

Consider that things are isotropic in that waves varying in direction about the origin, but always having the same $|\mathbf{k}| = k$, will have the same $\left\langle |A(\mathbf{k})|^2 \right\rangle$. And our integral in (29) is effectively an integral in $\mathbf{k}$ space of a continuum of spherical surfaces, where sub-integration is carried out over each surface and then those surface integrals are integrated in the radial direction. For each of these spherical surfaces, we can take $\left\langle |A(\mathbf{k})|^2 \right\rangle = \left\langle |A(k)|^2 \right\rangle$ and use the same orthogonality relation in $\mathbf{k}$ space as we used in (24) in $\mathbf{r}$ space, to get

$$C_l = \frac{2}{\pi}(-i)^{l'} i^l \int \left\langle |A(k)|^2 \right\rangle j_l(kr) j_{l'}(kr) Y_{l'm'}(\mathbf{n}_{\mathbf{k}}) Y_{lm}^*(\mathbf{n}_{\mathbf{k}}) \underbrace{\frac{d^3 k}{k^2 d\Omega\, dk}}$$

$$= \frac{2}{\pi}(-i)^{l'} i^l \int \left\langle |A(k)|^2 \right\rangle j_l(kr) j_{l'}(kr) \underbrace{\left(\int_\Omega Y_{l'm'}(\mathbf{n}_{\mathbf{k}}) Y_{lm}^*(\mathbf{n}_{\mathbf{k}}) d\Omega \right)}_{\delta_{ll'}\delta_{mm'}} k^2 dk \qquad (30)$$

[1] Abramo, L. Raul, and Pereira, Thiago S., Testing gaussiantity, homogeneity and isotropy with the cosmic microwave background, *Advances in Astronomy*, Vol. 2010, Article ID 378203, 25 pages. http://arxiv.org/abs/1002.3173. See (12) and the line after (17).

Or

$$C_l = \frac{2}{\pi}(-i)^l\, i^l \int \left\langle |A(k)|^2 \right\rangle j_l^2(kr) k^2\, dk = \frac{2}{\pi}\underbrace{(-1)^l\,(i^2)^l}_{(-1)^{2l}=1} \int \left\langle |A(k)|^2 \right\rangle j_l^2(kr) k^2\, dk \qquad . \qquad (31)$$

$$= \frac{2}{\pi} \int \left\langle |A(k)|^2 \right\rangle j_l^2(kr) k^2\, dk .$$

and thus, (31) is the relationship we sought between C_l and $A(\mathbf{k})$. Actually, it is a relationship between the variance in our spherical harmonic system and the variance in the Cartesian Fourier system. We will have a little more to say about this in Sect. 7.4

7 Plotting C_l vs l

7.1 Angular Variation

As shown in Appendix A, Sect. 11.5.7, pg. 38, the angular separation between variations, such as those shown in Fig. 8, for a given harmonic mode l, is

$$\text{angular variation} = \frac{180^{\text{o}}}{l} \qquad \left(= \frac{\pi}{l} \text{ in radians} \right) \qquad (32)$$

7.2 Peaks in Power Spectrum

It turns out that the fundamental standing wave (see Figs. 3 and 4, pgs. 3 and 3) of length L, via the mechanism depicted in Fig. 4, pg. 6, becomes a spherical harmonic with nodes separated by a little under 1°. In other words, the C_l for the CMB (see Fig. 1, pg. 1) peaks at about $l = 200$ or so.

We will discuss the meaning of this and the other peaks later on.

7.3 Background in Power Spectral Analysis Needed for Subsequent Material

In Appendix B, pg. 38, we present a simplified, introductory overview of power spectra and how they are derived from the wave amplitude (and wave variance). This information will be needed as a prerequisite for the following section. Some readers may already know that material. Some may not, or may be a bit rusty on it.

7.4 Why CMB Plots Have $l(l + 1)C_l/2\pi$ on the Vertical Axis Rather than C_l

The reason we see $l(l + 1)C_l/2\pi$ on the vertical axis of typical CMB power spectrum plots such as Fig. 1, pg. 1, has to do with our conversion from Fourier analyses in Cartesian coordinates to spherical harmonic analysis in spherical coordinates (Sect.6.2, pg.16) plus our desire to work with spectral power (rather than variance) plots having log scaling on the l axis.

The theory of inflation and subsequent expansion posit an effectively uniform (subject to subtleties) distribution of initial fluctuations in power across all wavelengths $\mathbf{k}$, i.e., scale invariance. On average, no fluctuation wavelength has an intrinsic, enhanced power over any others. The dynamics of acoustic wave formation change this, of course, but initially, before that got started, the whole thing was egalitarian.

Representing this initially democratic situation is rather straightforward in Cartesian space, where each Fourier component of wave vector $\mathbf{k}$ would be independent of all others. But this becomes less straightforward for spherical harmonics where each different spherical harmonic amplitude a_{lm} is a "funky" combination of the Fourier amplitude $A(\mathbf{k})$, as shown in (24).

As we will see, this funkiness of spherical harmonics can be modified in an advantageous way by multiplying each C_l by $l(l + 1)/2\pi$. For the case of a universe with no acoustic wave formation, this should give

us a curve in Fig. 1 of a straight horizontal line, subject to some subtleties beyond the scope of this discussion. So any changes via acoustic wave formation seen in our universe would show up in the figure as deviations from the horizontal line and "jump out" at us. They would not be submerged in other, unrelated variations with l due to the funkiness of spherical harmonics.

7.4.1 Relate C_l to the Temperature Power Spectrum in k

From Appendix B, pg. 38, relation (114) the Fourier <u>temperature power spectrum</u> $P_T(k)$ is, with a conventional choice of constant to turn the proportional sign to an equal sign,

$$P_T(k) = \frac{k^2}{2\pi^2} \left\langle \left| A(k) \right|^2 \right\rangle . \tag{33}$$

As also shown in Appendix B, relation (115), with symbols changed to k space below, shows how, given $P_T(k)$, we can determine the power over a given interval of a power spectrum,

$$\text{power between } k_1 \text{ and } k_2 = \int_{k_1}^{k_2} P_T(k) \, dk ,$$

where $P_T(k)$ is the power per unit k.

Solving (33) for $\left\langle \left| A(k) \right|^2 \right\rangle$ and inserting into (31) gives us

$$C_l = 4\pi \int P_T(k) j_l^2(kr) \, dk , \tag{34}$$

which relates the Fourier power spectrum $P_T(k)$, i.e., the power per unit k, in terms of C_l.

It is often desirable (and it is in CMB analysis) to work with the power per unit $\log k$, instead of the power per unit k. If we plot such a quantity and have a log scale for k on the horizontal axis, one can "eyeball" the power in an interval as simply the area one sees under the curve inside that interval.

To do this, we need to find an integrand for a relation parallel to (34) that is integrated with respect to $d(\log k)$. To find this integrand, reconfigure (34) as

$$C_l = 4\pi \int P_T(k) j_l^2(kr) k \underbrace{\frac{dk}{k}}_{d(\log k)} = 4\pi \int j_l^2(kr) \underbrace{k \, P_T(k)}_{\Delta_T^2(k)} d(\log k), \tag{35}$$

where we introduce the new symbol $\Delta_T^2(k)$. For this way of writing C_l, $\Delta_T^2(k) = k \, P_T(k)$ is power per unit $\log k$.

7.4.2 Evaluate the Integral for C_l with the Spherical Bessel Function in It

From integral tables, we find

$$\int j_l^2(z) \, d(\log z) = \frac{1}{2l(l+1)} . \tag{36}$$

From (36), therefore,

$$\begin{aligned}
\frac{1}{2l(l+1)} &= \int j_l^2(kr) \, d(\log kr) = \int j_l^2(kr) \frac{d(kr)}{kr} = \int j_l^2(kr) \frac{r \, dk}{kr} \\
&= \int j_l^2(kr) \frac{d(k)}{k} = \int j_l^2(kr) \, d(\log k) = \frac{1}{2l(l+1)} .
\end{aligned} \tag{37}$$

It is also known that a spherical Bessel function of order l peaks when its argument is approximately given by l, i.e., $j_l^2(kr)$ peaks at about $kr = l$. Further, this peak is very narrow with j_l effectively zero elsewhere. Hence,

over the integral of (35), only a narrow range of k contributes (around $k = l/r$), and over this range $\Delta_T^2(k)$ is approximately constant (and equal to $\Delta_T^2(k)(k = l/r)$.

Thus (35) becomes effectively

$$C_l \approx 4\pi \Delta_T^2(k = l/r) \underbrace{\int j_l^2(kr) d(\log k)}_{\substack{\text{only region near} \\ k=l/r \text{ contributes}}} . \tag{38}$$

With the last part of (37), we have

$$C_l \approx \frac{2\pi}{l(l+1)} \Delta_T^2(k = l/r). \tag{39}$$

7.4.3 Back to the Power Spectrum Plot

$\Delta_T^2(k)$ is the power spectrum per unit log k, for Fourier components in Cartesian coordinates. It is the number we really want to compare to our theory, which is grounded in Fourier analysis in Cartesian coordinates. So a log plot (or any other plot) of C_l (a spherical harmonics based number) vs l distorts our perspective on what the real physics is doing (which we grasp more readily in Cartesian coordinate form).

Thus, if we multiply (39) by $l(l + 1)/2\pi$, we get (approximately) $\Delta_T^2(k)$, our Fourier analysis friend that we feel more at home with.

$$\frac{l(l+1)}{2\pi} C_l \approx \Delta_T^2(k = l/r) \qquad \text{the number typically plotted on CMB vertical axis vs } l. \tag{40}$$

8 What the CMB Power Spectrum Tells Us

8.1 The First Peak

The first peak in Fig. 1, pg. 1, is at about $l \approx 200$ (a little less than 1°), which is related to the width L of a fundamental mode. (See Fig. 5, pg. 5.) The length L is the distance sound travels from just after the big bang to recombination. Cosmologists can calculate what that length should be. Knowing the distance to the LSS, they can then calculate what the angular separation (degrees, or equivalently the spherical mode number l) they would see. Note, from Fig. 9, that this angular measurement varies depending upon whether the universe is curved or not.

Flat Surface   Positive Curvature Surface
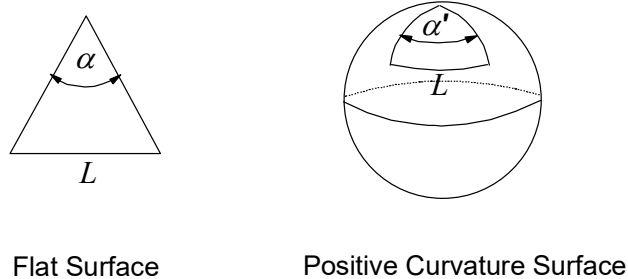
Figure 9. Measuring Angles Seen to Ends of a Length L

A viewer looking at the ends of a known length at a given distance away in a positively curved space measures a larger angle between the ends than a viewer of the same length and given distance away in a flat space. In Fig. 9, $\alpha < \alpha'$. A negatively curved space would have a smaller angle than a flat space.

For the CMB data, the angular measurement of L, the width of our fundamental mode, shows up as the location of the first peak, i.e., the l, value or equivalently the angle associated with that l value via (32). If the calculated value of that angle (l value) for a flat universe matches the CMB data location, we have a flat universe. If the measured angular value is larger (peak moves to the left, to lower l), we live in a positively curved universe; if smaller (peak moves to the right, to higher l), in a negatively curved one.

The data match for the peak location is, to fairly high accuracy, dead on for a flat universe.

Note that subtleties and uncertainties exist in the calculation and the measurement, and other parameters affect peak location to some degree as well, but higher peaks display the same dependence on curvature, so they can be used to check and refine the conclusions from the first peak. And for curvature, they check pretty well.

8.2 The Second Peak

From Fig. 1, we can see that the second acoustic peak is much lower than the first. To understand this, we need first to recognize, from Fig. 5, pg. 5, and related discussion, that the odd numbered peaks (first, third, etc) in the CMB power spectrum ($n = 1, 5, 9, …$ in Fig. 5) are, overall, compressive in nature. Even number peaks (second, fourth, etc.) in the spectrum ($n = 3, 7, …$ in Fig. 5) are, overall, rarefied in nature.

The oscillations result from massive baryons in more dense regions attracting more baryons with the resulting increase in baryons heating up the baryons and the photons they are in contact with. The photon pressure acts like spring to repel the baryons, so they spread and become less dense. After a time of expansion/rarefication the photon pressure decreases and gravity begins to pull baryons back closer together again. The whole process repeats leading to an oscillation that is analogous to a spring mass system. (See Fig. 10.) The mass in that system corresponds to baryon mass, the spring to photon pressure.
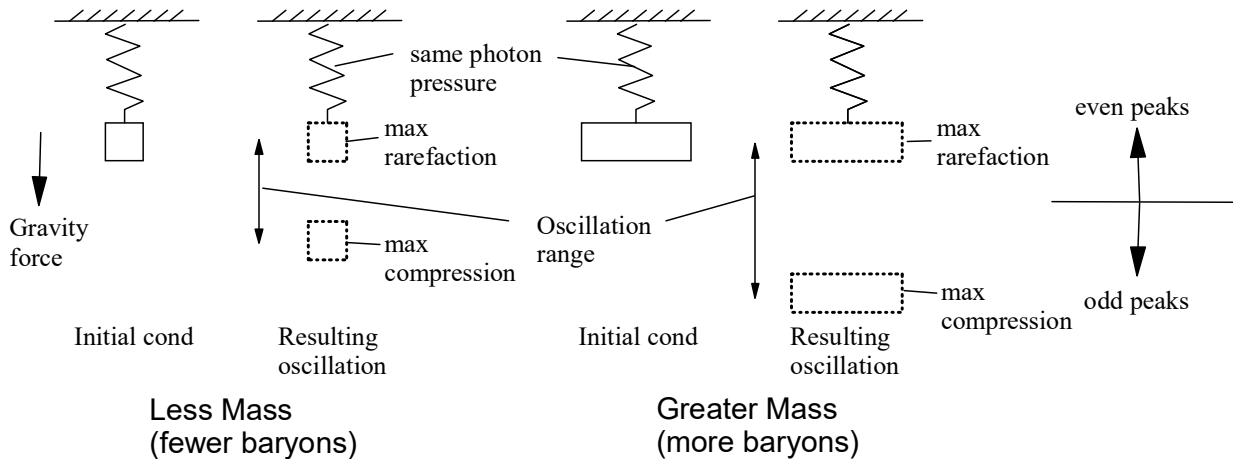
Figure 10. Analogy of Spring Mass Oscillation to Baryon Acoustic Wave Oscillation

Consider a given rarefied region, represented by the initial condition location in Fig. 10. With that same rarefied region, if there are more baryons in the adjacent denser region, the attraction will be greater, resulting in greater compression. A spring-mass system, like our BOAs, rebounds back to its initial condition (rarefied for BAOs) regardless of the extension (compressed fro BAOs). But the extension (compression) is greater for greater mass.

We know the odd numbered peaks represent overall compression; the even ones, overall rarefication. If we have greater mass (more baryons) the compression level will be greater, so the odd numbered peaks will be more pronounced (higher in our spectral density plot, as in Fig. 1). Thus, increasing baryon number in our universe will increase the height of the odd numbered peaks relative to the even numbered peaks. We see this effect in Fig. 1, where there is a general trend for peak height to reduce with increasing l. The first peak (compressive) is much higher than the second (rarefied), and the third peak is about as high as the second.

<u>The bottom line:</u> The relative heights of the odd and even numbered peaks reflect the baryon density. Cosmologists can, of course, quantify this to give us a precise value.

8.3   Higher Numbered Peaks and Parameter Determination

The heights, locations (l values), and shapes of the peaks in the CMB spectral density tell us a whole lot about the various parameters of our universe, such as curvature, baryon density, dark matter density, dark energy density, etc. In general, a given parameter can affect more than one peak. For example, curvature affects the location of all peaks.

Conversely, characteristics of a given peak can be affected by more than one parameter. For example, different baryon density means a different oscillation frequency (slower for more mass) for all standing waves. This will change the value (slightly, as it turns out) of l for each peak, including the first. So, what we said before about the first peak determining curvature has to be modified a bit. We also have to take into account the shift in l value due to baryon density. Again, cosmologists do this as part of the analysis of the CMB spectrum.

The above is an example of <u>degeneracy</u> in cosmological parameters, where we need additional information from other parts of the CMB spectrum to pin down a particular parameter.

Note that cosmologists use computer programs (see Sect. 10) to generate model CMB spectra. One inputs various parameters (dark energy percentage, baryon density, etc.) and the program spits out a power spectrum. By varying the parameters one gets a fit to the data and pins down which parameters yield that fit. See Fig. 11 for a graphic of what the CMB spectrum would look like for various values of certain parameters.
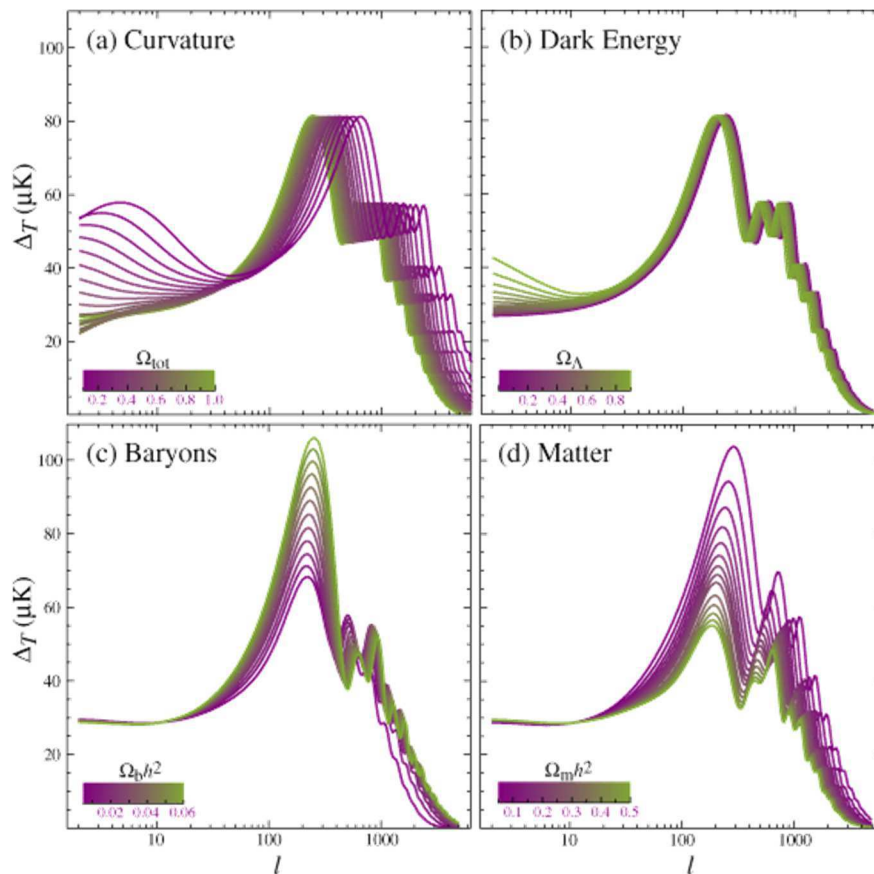
Figure 11. Plots of the CMB Spectrum for Different Values of Key Parameters
From webpage of Professors Hu and Dodelson http://background.uchicago.edu/~whu/araa/node15.html

From graphs such as those of Fig. 11, cosmologists have determined our universe is flat to high accuracy and has values for dark energy of about 69%, dark matter of about 26%, and ordinary (baryonic) matter of about 5%. The resulting model is called the <u>concordance model</u>, or the <u>ΛCDM model</u>. (for lambda cold dark matter, where lambda represents dark energy in cosmological constant form).

8.4   The Damping Tail

Note in Fig. 1 that the curve is damped at high l. The reason for this is that recombination did not happen instantly, but took some time, some thousands of years, to transpire. In other language, the LSS is not infinitesimal in thickness. So, the photons will scatter a few times during this transition period, rather than be released unscathed in one grand, fleeting moment to forever hold the patterns impressed on them by the BAOs.

If the average distance a photon travels is larger than the wavelength of the BAO at a given l, then the scattering will tend to smooth out the temperature contrasts at that l value, and thus any peaks at that l will be dampened. So, at shorter BAO wavelengths (higher l) power spectrum values will drop dramatically. And that is what we see in Fig. 1.

Other factors such as the baryon density (higher means more scattering of photons) affect the degree of damping. So precise determination of the degree of damping helps in pinning down key parameters.

9   Summary

We have explored the physical basis of baryonic acoustic oscillations in the early universe, and from that, developed the appropriate mathematics, at a relatively elementary level, that lead to the CMB power spectrum. We then showed, again at an elementary level, how that spectrum can be used to determine key cosmological parameters.

The presentation has been greater in depth than that of typical CMB popularization websites, yet markedly simpler and more rudimentary than that of typical cosmological textbooks. It has been intended to serve those with undergraduate, or better, backgrounds in physics, who are not (yet, or ever will be) specialists in the field.

10   Further Reading

Professor Whu at the University of Chicago does an excellent job of describing much of the material herein, with lots of graphics, on his website http://background.uchicago.edu/~whu/index.html. See also, Max Tegmark's page http://space.mit.edu/home/tegmark/cmb/pipeline.html. The math on those pages is not as extensive as that found herein, however.

For a next step, after this document, I recommend "Testing gaussianity, homogeneity and isotropy with the cosmic microwave background" by L. Raul Abarmo and Thiago S. Pereira (http://arxiv.org/abs/1002.3173). The math in that document is more advanced and more tersely presented than that herein.

Textbooks on the subject include *Modern Cosmology* by Scott Dodelson (Academic Press, 2003), *Physical Foundations of Cosmology* by Viatcheslav Mukhanov (Cambridge 2005), *The Cosmic Microwave Background* by Ruth Durrer (Cambridge, 2008) *Primordial Cosmology* by Patrick Peter and Jean-Philippe Uzan (Oxford, 2009). These books are quite advanced compared to the present document and represent entire graduate courses on the CMB. The present document is a good preliminary introduction to those texts.

To generate CMB power spectral plots yourself, with different parameters (for dark energy, dark matter, baryon density, curvature, etc) go to NASA's http://lambda.gsfc.nasa.gov/toolbox/tb_camb_ov.cfm .

11 Appendix A. Summary of Spherical Harmonics

A good reference for this material is Cahill[2]. What follows is only a summary and be useful primarily for those who have studied this before, but are a little rusty.

To get to spherical harmonics, we have to start with Legendre polynomials.

11.1 Legendre Polynomials

Introduction

We start by noting that any function $f(x)$ can be expressed as a Taylor power series expansion,

$$f(x) = \sum_{s=0}^{\infty} c_s x^s \qquad c_s = \frac{f^{(s)}(0)}{s!} \qquad f^{(s)} \text{ is } s^{th} \text{ derivative of } f. \qquad (41)$$

Legendre polynomials are of similar form,

$$P_n(x) = a_0 + a_1 x + a_2 x^2 + ... + a_n x^n = \sum_{i=0}^{n} a_i x^i, \qquad (42)$$

but are cut off after n terms and have the following normalization (which may seem strange at first but helps in the long run)

$$P_n(x=1) = 1 \qquad \rightarrow \qquad P_n(1) = a_0 + a_1 + a_2 + ... + a_n = 1, \qquad (43)$$

and orthogonality condition (note the interval of integration $-1 < x < 1$, which again is chosen because it eventually helps),

$$\int_{-1}^{1} P_n(x) x^m dx = 0 \qquad m < n. \qquad (44)$$

(44) says that each Legendre polynomial of order n is orthogonal (over the interval shown) to any monomial x^m, provided $m < n$.

Thus, the first few Legendre polynomials (you can check if they meet the criteria of (43) and (44)) are

$$P_0(x) = 1 \qquad\qquad P_3(x) = \frac{1}{2}\left(5x^3 - 3\right)$$

$$P_1(x) = x \qquad\qquad P_4(x) = \frac{1}{8}\left(35x^4 - 30x^2 + 3\right) \qquad . \qquad (45)$$

$$P_2(x) = \frac{1}{2}\left(3x^2 - 1\right) \qquad\qquad P_5(x) = \frac{1}{8}\left(63x^5 - 70x^3 + 15x\right)$$

In a plot, they look like Fig. A-1.

---

[2] Cahill, Kevin, *Physical Mathematics*, (Cambridge) 2013, pgs. 305-424.
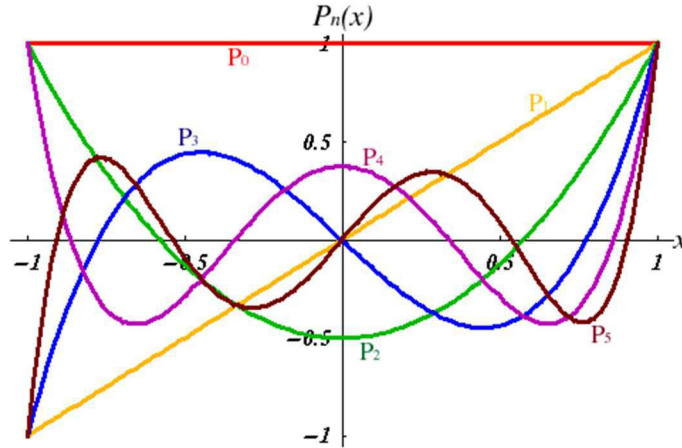
Figure A-1. Plots of the First Six Legendre Polynomials

There are shortcuts to finding Legendre polynomials called the Rodrigues formula ((8.8) pg. 306 of Cahill) and a recurrence relation ((8.38) of Cahill). The <u>Rodrigues formula</u> is

$$P_n(x) = \frac{1}{2^n n!} \frac{d^n (x^2 - 1)^n}{dx^n}, \tag{46}$$

which you can check to see gives the first few polynomials in (45).

<u>Helpful Way to Express Legendre Polynomials</u>

It turns out to help in many things in physics (as we will see shortly for one example), if we take the argument x for Legendre polynomials to be $\cos \theta$. That is, in (45) and (46),

$$\text{Take } x \to \cos \theta$$

$$P_0(\cos\theta) = 1 \qquad\qquad P_3(\cos\theta) = \frac{1}{2}\left(5\cos^3\theta - 3\right)$$

$$P_1(\cos\theta) = \cos\theta \qquad\qquad P_4(\cos\theta) = \frac{1}{8}\left(35\cos^4\theta - 30\cos^2\theta + 3\right) \tag{47}$$

$$P_2(\cos\theta) = \frac{1}{2}\left(3\cos^2\theta - 1\right) \qquad\qquad P_5(\cos\theta) = \frac{1}{8}\left(63\cos^5\theta - 70\cos^3\theta + 15\cos\theta\right)$$

$$P_n(\cos\theta) = \frac{1}{2^n n!} \frac{d^n \left(\cos^2\theta - 1\right)^n}{d\left(\cos\theta\right)^n}. \tag{48}$$

With this substitution $x \to \cos\theta$, the horizontal axis in Fig. A-1 would go from $\theta = \pi$ ($x = -1$) to $\theta = 0$ ($x = 1$) with the vertical axis located at $\theta = \pi/2$ ($x = 0$). $P_1(\cos\theta)$ vs θ would then look like a half cycle of a cosine curve. Higher order Legendre polynomials would then be trigonometric functions of θ (though a bit more complicated that the ones we usually deal with.)

The integration limits of the orthogonality relations (44) were taken knowing in advance that we would be using the substitution $x \to \cos\theta$. The 1 to -1 integration range for x corresponds to 0 to π (which, since that is the range of variation of the θ coordinate in polar coordinates, we are foreshadowing where we might eventually use these relations). See Fig. A-2 below.

11.2 Legendre Polynomials Involved in Solutions to Key Physics Equations

Legendre polynomials help us in solving some key problems in physics, but we have a few more steps to go to see how.

11.2.1 Special Cases of a General Case Type Equation

General Case Type Equation

A general from of second order equation one runs into in physics is

$$\nabla^2 f + \left(g(\mathbf{x})\right)f = 0 \tag{49}$$

where ∇^2 is the Laplacian and $g(\mathbf{x})$ is a general function of space. One example is the time independent Schroedinger equation with $f = \psi$,

$$-\frac{\hbar^2}{2\mu}\nabla^2\psi + V(\mathbf{x})\psi = E\psi \;\;\rightarrow\;\; \nabla^2\psi + \underbrace{\frac{2\mu}{\hbar^2}(E-V)}_{g(\mathbf{x})}\psi = 0. \tag{50}$$

Special Case, g = constant

A special case of (49), where $g(\mathbf{x})$ is a constant (equal to k^2 below), is referred to as the Helmholtz equation,

$$\nabla^2 f + k^2 f = 0. \tag{51}$$

The solutions to the Helmholtz equation are spatial (static) waves. So one should (rightfully) consider the spatial oscillations in the CMB could be described mathematically by the solutions to it. More on this later.

Note that (51) can be expressed in Cartesian or spherical coordinates (or any other coordinates, though we won't be concerned with those others). In Cartesian coordinates, (51) has solutions of form

$$f(x) \propto sin\,kx,\; cos\,kx,\; \text{or}\; e^{ikx}\left(= cos\,kx + i\,sin\,kx\right)\quad \text{1D case}. \tag{52}$$

Special Case $g = 0$

For $g = 0$, we have the Laplace equation. For $f = \Phi$, the electric potential in a region free of charge, is a key relation for electrostatics. For Newtonian gravity, $f = \Phi$ would represent the gravitational field in a region free of mass.

Laplace eq (e.g., electric potential in region of zero charge) $\quad \nabla^2\Phi = 0 \;\;\left(\text{where } g = 0\right)$ (53)

Special Case, Spherical Coordinates with $g = g(r)$

Cases where (49) has g dependence only on the radial distance r from the origin of the coordinate system used,

$$\nabla^2 f + g(r)f = 0, \tag{54}$$

are common. One example is the Schroedinger equation applied to the hydrogen atom, comprising an electron in the field of a proton's coulomb potential $V(r) = e^2/4\pi r$.

Schroedinger eq, H atom $\quad -\dfrac{\hbar^2}{2\mu}\nabla^2\psi + V(r)\psi = E\psi \;\;\rightarrow\;\; \nabla^2\psi + \underbrace{\dfrac{2\mu}{\hbar^2}(E-V)}_{g(r)}\psi = 0$ (55)

For problems of this type, spherical coordinates work best, and we express ∇^2 in terms of $r,\;\theta,$ and ϕ.
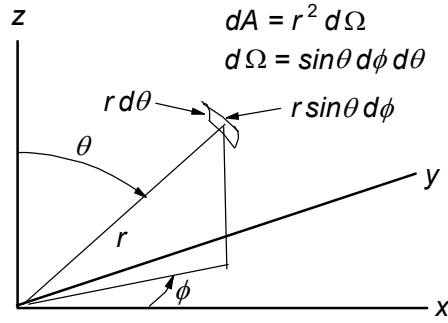
Figure A-2. Spherical Coordinates with Differential Solid Angle $d\Omega$ Shown

Special Case, Spherical Coordinates on 2D Surface of Sphere

If we wish to examine behavior of something on the surface of a sphere (such as the CMB radiation), we can fix r in (54), and examine the resulting solution. That solution would have functional dependence only on θ and ϕ. In effect, $g(r)$ = const in (54), and we would essentially be solving the Helmholtz equation (the equation for spatially varying static waves) on the surface of the sphere.

We should expect f in this case to parallel the solutions to the Schroedinger equation for the hydrogen atom with respect to behavior with respect to θ and ϕ. This should help most readers follow the remaining parts of this appendix, since most have some familiarity with that problem.

11.2.2 Solving the 2D Surface of a Sphere Case

Separation of Variables to Solve g(r) Case

In cases where g is a symmetric function of r (purely a function of r and not θ or ϕ), then the problem of solving (49) simplifies. We try a separation of variables approach, i.e., we separate f into functions dependent on r, θ, and ϕ, as follows.

$$f(r,\theta,\phi) = R(r)\underbrace{\Theta(\theta)\Phi(\phi)}_{Y(\theta,\phi)} = R(r)Y(\theta,\phi) \qquad \text{works for } g = \text{ only a function of } r \quad (56)$$

We then substitute (56) into (54), where ∇^2 is expressed in spherical coordinates. When we do this (again, this is a summary review, we aren't going through all the steps), we find the following three separated equations, each only involving one coordinate.

$$\frac{1}{R}\frac{d}{dr}\left(r^2\frac{dR}{dr}\right) + g(r)r^2 = l(l+1) \qquad (l \text{ an integer. See why below.}) \qquad \underline{\text{Radial equation}} \quad (57)$$

$$\frac{d^2\Phi}{d\phi^2} + m^2\Phi = 0 \qquad \left(\begin{array}{l} m \text{ an integer and } -l \le m \le l. \text{ See why below.} \\ \text{This is actually Helmholtz eq with } x \to \phi. \end{array}\right) \qquad (58)$$

$$\frac{1}{\sin\theta}\frac{d}{d\theta}\left(\sin\theta\frac{d\Theta}{d\theta}\right) + \left(l(l+1) - \frac{m^2}{\sin^2\theta}\right)\Theta = 0 \qquad \underline{\text{associated Legendre equation}} \quad (59)$$

Using separation of variables we have converted a partial differential equation in three variables, which is generally very difficult to solve, into three separate ordinary differential equations, each in only a single function dependent on a single independent variable.

Radial Equation (not needed for CMBR analysis)

While we will ignore (57), as we are only dealing with functions on a spherical surface (at constant r), we note that it gives rise in QM to the radial part of the hydrogen atom wave function and in doing so, the fundamental energy eigenvalues.[3]

Φ Equation

The Helmholz equation in ϕ, (58), is readily solved as

$$\Phi_m(\phi) = \frac{e^{im\phi}}{\sqrt{2\pi}} \qquad \text{One solution for each value of integer } m., \qquad (60)$$

where the constant of the denominator is chosen so Φ is appropriately normalized (over $0 \le \phi \le 2\pi$). Note (60) expresses a (complex) wave oscillation as one progresses in the ϕ direction. We stated in (58) that m must be an integer. The reason is that its solution (60) can only be single valued (as one progresses around ϕ past 360º), if m is an integer. The number of nodes in 360º increases directly with m.

Associated Legendre Equation

There is a fair amount of algebra involved in determining $\Theta(\theta)$ of (59), the associated Legendre equation, but we cut to the chase here. For each different l and each different m, there is a separate solution to (59), which we label as Θ_{lm}. These <u>solutions are</u> proportional to entities called the <u>associated Legendre polynomials,</u> labeled as <u>P_{lm}</u>, which are closely related to Legendre polynomials. Thus, where we will later choose the proportionality constant to suit out needs, (59) can be re-written

$$\text{for } \Theta_{lm} = (\text{constant}) P_{lm} \text{ , as}$$

$$\frac{1}{\sin\theta}\frac{d}{d\theta}\left(\sin\theta\frac{dP_{lm}}{d\theta}\right) + \left(l(l+1) - \frac{m^2}{\sin^2\theta}\right)P_{lm} = 0 \qquad \left(\begin{array}{l} P_{lm} \text{ is } \underline{\text{associated Legendre polynomial}} \\ \text{that solves associated Legendre equation} \end{array}\right).(61)$$

If one goes through the math (see Cahill, we are only summarizing), one finds P_{lm} in (61) to be (where we use the symbol "l" in place of "n" in the Legendre polynomial symbol)

$$\underbrace{P_{lm}}_{\substack{\text{associated}\\ \text{Legendre}\\ \text{polynomial}}} = \sin^m\theta \frac{d^m}{d\cos^m\theta}\underbrace{P_l(\cos\theta)}_{\substack{\text{Legendre}\\ \text{polynomial}\\ x\to\cos\theta}} \qquad (l \text{ and } m \text{ integers with } -l \le m \le l). \qquad (62)$$

The solutions to (61) are related to our earlier discussed Legendre polynomials via (62) where we take $x \to \cos\theta$, as discussed in Sect. 11.1. We note that it is common in the literature to write the argument of P_{lm} as $\cos\theta$ instead of θ. In that case, (62) becomes

$$P_{lm}(\cos\theta) = \left(1-\cos^2\theta\right)^{m/2}\frac{d^m}{d\cos^m\theta}P_l(\cos\theta) \qquad (l \text{ and } m \text{ integers with } -l \le m \le l). \qquad (63)$$

You can check that the first few Legendre polynomials in (47), used in (63), actually solve (61).

---

[3] Note that for the special case $g(r) =$ constant (54) becomes the Helmholtz equation, and we have a different radial equation (57). For that constant equal to zero, $g(r) = 0$, (54) becomes the Laplace equation, with yet a different radial equation. However the angular dependent equations (58) and (59) are the same for $g(r)$ isotopic or constant (whether that constant is zero or not). Thus, in the discussion that follows regarding the solutions to (58) and (59), all conclusions are the same for the 3D spherical forms of each of the Helmholtz equation (51), the Laplace equation (53), the hydrogen atom Schroedinger equation (55), any case with isotropic $g(\mathbf{x})$ (54), and any case on the 2D surface of a sphere (like the CMB analysis). In the literature, one sometimes reads that the solution forms we are about to explore (associated Legendre polynomials, in particular) are derived from the Laplace equation, and sometimes from the Helmholtz equation or general isotropic form for g. Hopefully, this footnote will avoid confusion when you run into such statements.

Using Rodrigues formula (46) (with $x \to \cos\theta$) in (63), we get

$$P_{lm}(\cos\theta) = \left(1 - \cos^2\theta\right)^{m/2} \frac{d^m}{d\cos^m\theta} \frac{1}{2^l\, l!} \frac{d^l\left(\cos^2\theta - 1\right)^l}{d\left(\cos\theta\right)}$$

$$= \frac{1}{2^l\, l!}\left(1 - \cos^2\theta\right)^{m/2} \frac{d^{m+l}\left(\cos^2\theta - 1\right)^l}{d\cos^{m+l}\theta}.$$

(64)

The bottom row of (64) only makes sense if $m + l \geq 0$ with $m + l$ an integer. Since m is an integer (see above), then l must be. Further, if m exceeds l, then any derivative in that bottom row will yield zero for P_{lm}. Thus, we justify what was stated in (57), (58), (62), and (63) about l and m.

When all is said and done, the first several associated Legendre polynomials, found via (64), look like

$$P_{00} = 1 \qquad P_{10} = \cos\theta \qquad P_{20} = \frac{1}{2}\left(3\cos^2\theta - 1\right) \qquad P_{30} = \frac{1}{2}\cos\theta\left(5\cos^2\theta - 3\right)$$

$$P_{11} = -\sin\theta \qquad P_{21} = -3\sin\theta\cos\theta \qquad P_{31} = -\frac{3}{2}\sin\theta\left(5\cos^2\theta - 1\right)$$

$$P_{22} = 3\sin^2\theta \qquad P_{32} = 15\cos\theta\sin^2\theta \qquad (65)$$

$$P_{33} = -15\sin^3\theta$$

$$\text{where} \quad P_{l-m} = (-1)^m \frac{(l-m)!}{(l+m)!} P_{lm}\,.$$

To check, and strengthen one's understanding, any of (65) can be inserted into (61) to verify that they are indeed solutions to the associated Legendre equation.

11.3 Completeness and Orthonormality of $P_l{}^m$

11.3.1 Completeness

Other than arbitrary constants by which they could be multiplied, all possible solutions to the associated Legendre equation are included in P_{lm} of (63), so the set of those solutions shown there spans the space of all possible solutions over θ. This is similar to the 1D spatial (static) wave (Helmholtz) equation (51) where the set of all e^{ik_nx}, where $k_n = n2\pi/L$ spans the space of all solutions to that equation over the interval treated.

Further, we know from the Fourier theorem that the solutions e^{ik_nx} span the space of *all* possible functions of x over the interval, not just functions that are specific solutions to the Helmholtz equation. Similarly, the associated Legendre polynomials $P_{lm}(\cos\theta)$ span the space of all possible functions of θ, not simply those that are solutions to the associated Legendre equation.

Thus, the set $\underline{P_{lm}}(\cos\theta)$ is complete over θ. Any possible function of θ can be shown equal to a sum of a_{lm} $\underline{P_{lm}}(\cos\theta)$ over all l and m, where the constant coefficient $a_{l'm'}$ represents how much of $P_{l'm'}$ is present. For example, in the $m = 0$ case (no variation in the ϕ direction since $e^{im\phi} = 1$ for $m = 0$), any function purely of θ (and not ϕ) can be represented as

$$f(\theta) = a_{00}P_{00}(\cos\theta) + a_{10}P_{10}(\cos\theta) + a_{20}P_{20}(\cos\theta) + \ldots = \sum_{l=0}^{\infty} a_{l0}P_{l0}(\cos\theta) \qquad m = 0. \qquad (66)$$

11.3.2 Orthonormality

<u>For same *m*</u>

We first state, then shortly after that prove, the orthogonality of $\underline{P_{lm}}$ which have the same *m*, but different *l*. Note that since $\underline{P_{lm}}$ is real (see (65), for examples), we do not need to take the complex conjugate of $\underline{P_{lm}}$ times $\underline{P_{lm}}$, as is done, for example, with quantum wave functions.

$$\int_{-1}^{1} P_{l'm}(x) P_{lm}(x) dx = 0 \qquad l \neq l', \text{ same } m, \ x = \cos\theta \ . \tag{67}$$

The inner product of $\underline{P_{lm}}$ with itself (same *m* and same *l*) represents the normalization and is (reference to proof given below)

$$\int_{-1}^{1} P_{l'm}(x) P_{lm}(x) dx = \frac{2}{2l+1} \frac{(l+m)!}{(l-m)!} \qquad \text{same } l, \text{ same } m, \ x = \cos\theta \ . \tag{68}$$

We can combine (67) and (68), and substitute $\cos\theta$ for *x*, to yield the <u>orthonormality condition for P_{lm}</u>

$$\int_{-1}^{1} P_{l'm}(x) P_{lm}(x) dx = \frac{2}{2l+1} \frac{(l+m)!}{(l-m)!} \delta_{ll'} \quad = \quad \int_{\pi}^{0} P_{l'm}(\cos\theta) P_{lm}(\cos\theta) d(\cos\theta) = -\int_{\pi}^{0} P_{l'm}(\cos\theta) P_{lm}(\cos\theta) \sin\theta d\theta$$

$$= \int_{0}^{\pi} P_{l'm}(\cos\theta) P_{lm}(\cos\theta) \sin\theta d\theta = \frac{2}{2l+1} \frac{(l+m)!}{(l-m)!} \delta_{ll'} . \qquad \text{same } m \tag{69}$$

<u>For different *m*</u>

On pg. 319, Cahill derives the orthonormality relations for the $\underline{P_{lm}}$, for different *m*, but, as we will see, we will not need these.

<u>Proof of (67)</u>

To prove the orthogonality condition (67), we start by rearranging (61),

$$\frac{1}{\sin\theta} \frac{d}{d\theta} \left(\sin\theta \frac{dP_{lm}(\cos\theta)}{d\theta} \right) - \frac{m^2}{\sin^2\theta} P_{lm}(\cos\theta) = l(l+1) P_{lm}(\cos\theta) \qquad \begin{array}{l}\text{associated Legendre} \\ \text{equation, rearranged.}\end{array} \tag{70}$$

If we consider *m* fixed, then (70) can be considered an eigenvalue problem with eigenfunctions $\underline{P_{lm}}$ and eigenvalues $l(l+1)$. Eigenfunctions are always orthogonal. Thus, for integration over the stated interval, we have (67).

<u>Proof of (68)</u>

If I have time, I may someday write out the proof of (68), which I never actually looked at myself before writing this. (I had simply accepted the result, like one accepts integral formulas in a table without working them through oneself.) For now I simply note that it is only algebra, comprising substitution of the last line of (64) with $\cos\theta \rightarrow x$ into the LHS of (68) and working it all out. The full proof can be found in Arfken and Weber[4]. Cahill merely states the result (69) without proof.

11.4 Completeness and Orthonormality of $Y_l^m(\theta,\phi)$

11.4.1 Completeness

We have realized that $\underline{P_{lm}}$ is complete over θ for the interval 0 to π. Using similar logic as we had with the 1D Helmholtz equation (51) and its solutions being complete (spanning the space of all functions over *x*), the

---

[4] Arfken, George B., and Weber, Hans J., *Mathematical Methods for Physicists* (Academic Press, San Diego) 1995, pgs. 726-727.

solutions $e^{im\phi}$ to equation (58) (identical in form to the Helmholtz equation) are complete over ϕ for the interval 0 to 2π. Thus, from (56), where we now realize we need the l and m sub/superscripts,

$$Y_{lm}(\theta,\phi) = \Theta_{lm}(\theta)\Phi_m(\phi) = (\text{constant})P_{lm}(\cos\theta)\frac{e^{im\phi}}{\sqrt{2\pi}} \qquad \text{no sum on } m \qquad (71)$$

is complete over the 2D space defined by $0 \le \theta \le \pi$ and $0 \le \phi \le 2\pi$. Any function of θ and ϕ can be described by a sum over l and m of terms $a_{lm} Y_{lm}$, where the a_{lm} are appropriate constants.

11.4.2 Orthonormality

Normalization

Using (71), integrating $\left|Y_{lm}(\theta,\phi)\right|^2$ over all θ and ϕ (effectively integrating over the surface of a sphere with radius $r = 1$ in Fig. A-2 pg. 27), and normalizing by setting the result equal to unity, we have

$$1 = \oint Y_{lm}^*(\theta,\phi)Y_{lm}(\theta,\phi)d\Omega = \int_0^{2\pi}\int_0^{\pi} Y_{lm}^*(\theta,\phi)Y_{lm}(\theta,\phi)\sin\theta d\theta d\phi \qquad (\text{no sum on } m)$$

$$= \int_0^{2\pi}\int_0^{\pi} \Theta_{lm}^*(\theta)\Phi_m^*(\phi)\Theta_{lm}(\theta)\Phi_m(\phi)\sin\theta d\theta d\phi$$

$$= \int_0^{2\pi}\int_0^{\pi} |\text{constant}|^2 P_{lm}(\cos\theta)P_{lm}(\cos\theta)\frac{e^{-im\phi}}{\sqrt{2\pi}}\frac{e^{im\phi}}{\sqrt{2\pi}}\sin\theta d\theta d\phi \qquad (72)$$

$$= |\text{constant}|^2 \int_0^{\pi} P_{lm}(\cos\theta)P_{lm}(\cos\theta)\sin\theta d\theta \underbrace{\frac{1}{2\pi}\int_0^{2\pi} d\phi}_{=1}$$

$$= |\text{constant}|^2 \int_0^{\pi} P_{lm}(\cos\theta)P_{lm}(\cos\theta)\sin\theta d\theta.$$

From the last line of (69), with the last line of (72) equal to one, we see

$$|\text{constant}|^2 = \frac{2l+1}{2}\frac{(l-m)!}{(l+m)!}. \qquad (73)$$

Thus, from (71) we see the spherical harmonics are

$$\boxed{Y_{lm}(\theta,\phi) = \sqrt{\frac{2l+1}{2}\frac{(l-m)!}{(l+m)!}}\, P_{lm}(\cos\theta)\frac{e^{im\phi}}{\sqrt{2\pi}} \qquad \text{no sum on } l \text{ or } m.} \qquad (74)$$

Our normalization constant is the quantity inside the square root sign above.

Orthogonality

For the same m and $l' \ne l$

From (69), we see that for the same m and any $l' \ne l$, $P_{l'm}$ and $\underline{P_{lm}}$ are orthogonal over θ. Thus, $Y_{l'm}$ and Y_{lm} must also be orthogonal over an entire sphere, i.e.,

$$\int_0^{2\pi}\int_0^{\pi} Y_{l'm}^*(\theta,\phi)Y_{lm}(\theta,\phi)\sin\theta d\theta d\phi \qquad \left(\text{no sum on } m, \ l'\neq l\right)$$

$$=\int_0^{2\pi}\int_0^{\pi} \frac{2l+1}{2}\frac{(l-m)!}{(l+m)!}P_{l'm}(\cos\theta)P_{lm}(\cos\theta)\frac{e^{-im\phi}}{\sqrt{2\pi}}\frac{e^{im\phi}}{\sqrt{2\pi}}\sin\theta d\theta d\phi \qquad (75)$$

$$=\frac{2l+1}{2}\frac{(l-m)!}{(l+m)!}\underbrace{\int_0^{\pi} P_{l'm}(\cos\theta)P_{lm}(\cos\theta)\sin\theta d\theta}_{=\ 0\ \text{for}\ l'\neq l}=0\ .$$

(75) tells us that for the same m and $l'\neq l$, the spherical harmonics are orthogonal.

For different m' and m and any l and l'

For different m' and m, regardless of l' and l, we have

$$\int_0^{2\pi}\int_0^{\pi} Y_{l'm'}^*(\theta,\phi)Y_{lm}(\theta,\phi)\sin\theta d\theta d\phi \qquad \left(m'\neq m,\ l'\text{ and }l\text{ may be same or different}\right)$$

$$=\int_0^{2\pi}\int_0^{\pi}\sqrt{\frac{2l'+1}{2}\frac{(l'-m')!}{(l'+m')!}}\sqrt{\frac{2l+1}{2}\frac{(l-m)!}{(l+m)!}}P_{l'm'}(\cos\theta)P_{lm}(\cos\theta)\frac{e^{-im'\phi}}{\sqrt{2\pi}}\frac{e^{im\phi}}{\sqrt{2\pi}}\sin\theta d\theta d\phi$$

(76)

$$=\sqrt{\frac{2l'+1}{2}\frac{(l'-m')!}{(l'+m')!}}\sqrt{\frac{2l+1}{2}\frac{(l-m)!}{(l+m)!}}\left(\int_0^{\pi} P_{l'm}(\cos\theta)P_{lm}(\cos\theta)\sin\theta d\theta\right)\frac{1}{2\pi}\underbrace{\int_0^{2\pi} e^{im'\phi}e^{-im\phi}d\phi}_{=\ 0\ \text{for}\ m'\neq m}$$

$$=0.$$

(76) tells us that any two spherical harmonics with different m values are orthogonal.

For the same m and l

$$\int_0^{2\pi}\int_0^{\pi} Y_{lm}^*(\theta,\phi)Y_{lm}(\theta,\phi)\sin\theta d\theta d\phi \qquad \left(m\text{ and }l\text{ the same, no sum on them}\right)$$

$$=\int_0^{2\pi}\int_0^{\pi}\sqrt{\frac{2l+1}{2}\frac{(l-m)!}{(l+m)!}}P_{lm}(\cos\theta)P_{lm}(\cos\theta)\frac{e^{im\phi}}{\sqrt{2\pi}}\frac{e^{im\phi}}{\sqrt{2\pi}}\sin\theta d\theta d\phi$$

(77)

$$=\sqrt{\frac{2l+1}{2}\frac{(l-m)!}{(l+m)!}}\underbrace{\left(\int_0^{\pi} P_{l'm}(\cos\theta)P_{lm}(\cos\theta)\sin\theta d\theta\right)}_{\sqrt{\frac{2}{2l+1}\frac{(l+m)!}{(l-m)!}}}\underbrace{\frac{1}{2\pi}\int_0^{2\pi} e^{im\phi}e^{-im\phi}d\phi}_{=1}$$

$$=1.$$

(77) tells us that the inner product of a spherical harmonic with itself equals one. This is our normalization for spherical harmonics.

Bottom line: Two spherical harmonics are orthogonal (inner product over a spherical surface is zero) unless both have the same l and m. In that case the normalization is given by (78) with $m'=m$ and $l'=l$.

$$\boxed{\int_0^{2\pi}\int_0^{\pi} Y_{l'm'}^*(\theta,\phi)Y_{lm}(\theta,\phi)\sin\theta\,d\theta\,d\phi=\delta_{ll'}\delta_{m'm}\quad\begin{array}{l}\text{Spherical harmonics}\\\text{orthonormality condition}\end{array}} \qquad (78)$$

11.5 Expanding a Function of θ and ϕ in Y_{lm}

11.5.1 The Expansion

Since the spherical harmonics are complete, we can expand any smooth function $f(\theta,\phi)$ in terms of them.

$$f(\theta,\phi) = \sum_{l=0}^{\infty} \sum_{m=-l}^{l} a_{lm} Y_{lm}(\theta,\phi) . \tag{79}$$

Noting that

$$\int_0^{2\pi} \int_0^{\pi} Y_{l'm'}^*(\theta,\phi) f(\theta,\phi) \sin\theta \, d\theta \, d\phi = \int_0^{2\pi} \int_0^{\pi} Y_{l'm'}^*(\theta,\phi) \left(\sum_{l=0}^{\infty} \sum_{m=-l}^{l} a_{lm} Y_{lm}(\theta,\phi) \right) \sin\theta \, d\theta \, d\phi$$

$$= \sum_{l=0}^{\infty} \sum_{m=-l}^{l} a_{lm} \int_0^{2\pi} \int_0^{\pi} Y_{l'm'}^*(\theta,\phi) Y_{lm}(\theta,\phi) \sin\theta \, d\theta \, d\phi = \sum_{l=0}^{\infty} \sum_{m=-l}^{l} a_{lm} \delta_{ll'} \delta_{m'm} = a_{l'm'}, \tag{80}$$

we realize that we can find all a_{lm} for any $f(\theta,\phi)$ via

$$a_{lm} = \int_0^{2\pi} \int_0^{\pi} Y_l^{\dagger m}(\theta,\phi) f(\theta,\phi) \sin\theta \, d\theta \, d\phi. \tag{81}$$

11.5.2 Note for $m \to -m$

Note from (65),

$$P_{l-m} = (-1)^m \frac{(l-m)!}{(l+m)!} P_{lm}. \tag{82}$$

Using (74) with $m \to -m$, incorporating (82), and recalling that P_{lm} is real, we find

$$Y_{l-m}(\theta,\phi) = \sqrt{\frac{2l+1}{2} \frac{(l+m)!}{(l-m)!}} \, P_{l-m}(\cos\theta) \frac{e^{-im\phi}}{\sqrt{2\pi}} \qquad \text{no sum on } l \text{ or } m$$

$$= \sqrt{\frac{2l+1}{2} \frac{(l+m)!}{(l-m)!}} (-1)^m \frac{(l-m)!}{(l+m)!} P_{lm}(\cos\theta) \frac{e^{-im\phi}}{\sqrt{2\pi}} = (-1)^m \sqrt{\frac{2l+1}{2} \frac{(l-m)!}{(l+m)!}} \, P_{lm}(\cos\theta) \frac{e^{-im\phi}}{\sqrt{2\pi}} \tag{83}$$

$$= (-1)^m Y_{lm}^*(\theta,\phi).$$

11.5.3 Ramifications of $m \to -m$ Result

In our summation (79), for every spherical harmonic term $a_{lm} Y_{lm}$ there is a corresponding term

$$a_{l-m} Y_{l-m} = (-1)^m a_{l-m}^* Y_{lm}^*. \tag{84}$$

So, with appropriate choice of relation between a_{lm} and a_{l-m}, i.e.,

$$a_{lm} = (-1)^m a_{l-m}^* = \text{ real number}, \tag{85}$$

the m and $-m$ terms summed would be real for a given l. That is,

$$a_{lm} Y_{lm} + a_{l-m} Y_{l-m} = a_{lm} Y_{lm} + \underbrace{(-1)^m a_{l-m}^*}_{a_{lm}} Y_{lm}^* = a_{lm}\left(Y_{lm} + Y_{lm}^*\right) = \text{ real function} \qquad (\text{no sum on } l \text{ or } m). \tag{86}$$

Also, for $m = 0$, Y_{l0} is real. See (74) and recognize that P_{lm} is real for any m.

Bottom line: f in (79) can represent a real number (such as temperature of the CMB) even though the Y_{lm} are complex.

11.5.4 Comparing to Fourier Analysis in the Cartesian Case

We can compare the representation of a function of θ in terms of a series of associated Legendre polynomials to the representation of a function of the Cartesian coordinate x in terms of as series of sines and/or cosines (or equivalently, the real and/or imaginary part of e^{ikx}). Before doing so, we recall some trigonometric relations we will use along the way.

$$\sin^2\theta = \tfrac{1}{2}(1-\cos 2\theta) \quad (a) \qquad \cos^2\theta = \tfrac{1}{2}(1+\cos 2\theta) \quad (b) \qquad \sin\theta\cos\theta = \tfrac{1}{2}(\sin 2\theta) \quad (c) \qquad (87)$$

$$\sin^3\theta = \tfrac{1}{4}(3\sin\theta - \sin 3\theta) \qquad (a) \qquad \cos^3\theta = \tfrac{1}{4}(3\cos\theta + \cos 3\theta) \qquad (b)$$
$$\cos\theta\cos 2\theta = \tfrac{1}{2}(\cos\theta + \cos 3\theta) \qquad (c) \qquad \sin\theta\cos 2\theta = \tfrac{1}{2}(\sin 3\theta - \sin\theta) \qquad (d) \qquad (88)$$

Now take (79) with $\phi = 0$, i.e., consider $f = f(\theta)$, and insert (74).

$$f(\theta) = \sum_{l=0}^{\infty}\sum_{m=-l}^{l} a_{lm}Y_{lm}(\theta,\phi=0) = \sum_{l=0}^{\infty}\sum_{m=-l}^{l} \underbrace{a_{lm}\sqrt{\frac{2l+1}{2}\frac{(l-m)!}{(l+m)!}}}_{a'_{lm}} P_{lm}(\cos\theta) = \sum_{l=0}^{\infty}\sum_{m=-l}^{l} a'_{lm}\, P_{lm}(\cos\theta) \,. (89)$$

Compare this to a typical Fourier series expression for a function $h(x)$,

$$h(x) = \sum_{n=0}^{\infty} (a_n \cos nx + b_n \sin nx) \qquad (90)$$

Now look at (65) (repeated below for convenience) to see what some of the associated Legendre polynomials used in (89) look like.

$$P_{00} = 1 \qquad P_{10} = \cos\theta \qquad P_{20} = \frac{1}{2}(3\cos^2\theta - 1) \qquad P_{30} = \frac{1}{2}\cos\theta(5\cos^2\theta - 3)$$

$$P_{11} = -\sin\theta \qquad P_{21} = -3\sin\theta\cos\theta \qquad P_{31} = -\frac{3}{2}\sin\theta(5\cos^2\theta - 1)$$

$$P_{22} = 3\sin^2\theta \qquad P_{32} = 15\cos\theta\sin^2\theta \qquad (65)$$

$$P_{33} = -15\sin^3\theta$$

$$\text{where} \quad P_{l-m} = (-1)^m \frac{(l-m)!}{(l+m)!} P_{lm} \,.$$

We then convert (65) using (87) and (88) to get

$$P_{00} = 1 \qquad P_{10} = \cos\theta \qquad P_{20} = \tfrac{1}{2}(3\cos^2\theta - 1) = \tfrac{1}{2}\left(3\left(\tfrac{1}{2}(1+\cos 2\theta)\right)-1\right) = \tfrac{1}{4} + \tfrac{3}{4}\cos 2\theta$$

$$P_{11} = -\sin\theta \qquad P_{21} = -3\sin\theta\cos\theta = -\tfrac{3}{2}(\sin 2\theta)$$

$$P_{22} = 3\sin^2\theta = \tfrac{3}{2} - \tfrac{3}{2}\cos 2\theta$$

$$(91)$$

$$P_{30} = \tfrac{1}{2}\cos\theta(5\cos^2\theta - 3) = \tfrac{1}{2}\cos\theta\left(5\left(\tfrac{1}{2}(1+\cos 2\theta)\right)-3\right) = -\tfrac{7}{4}\cos\theta + \tfrac{5}{4}\cos\theta\cos 2\theta$$

$$= -\tfrac{14}{8}\cos\theta + \tfrac{5}{8}(\cos\theta + \cos 3\theta) == -\tfrac{9}{8}\cos\theta + \tfrac{5}{8}\cos 3\theta$$

P_{31}, P_{32}, P_{33} similarly yield expressions in $\cos\theta,\ \sin\theta,\ \cos 3\theta$, and $\sin 3\theta$.

The point is that terms in $\underline{P_{lm}}$ of order l have highest order exponents in both sine and cosine factors combined of l as shown in (65). These can be converted, as shown in (91), into expressions having terms with

only sine and/or cosine of angles $l\theta$ (l times θ) not raised to any power. But those are exactly the kinds of terms we find in (90), for $l \rightarrow n$ and $\theta \rightarrow x$.

In essence, the summation (89) is the same summation as (90). For example, for the $a_3\cos3x$ term in (90), we would have a comparable term in (89) $c_3\cos3\theta$, where the c_3 is a combination of different a_{lm}. Each term in (90) has a corresponding term (when we add together all the appropriate a_{lm} in the right way) in (89).

<u>Bottom Line:</u> The sum of all spherical harmonics in θ to yield a given function is effectively the same thing as a Fourier series summation of sines and cosines to yield the same function.

<u>2nd Bottom Line</u>: From (91), we see that the order l of a spherical harmonic indicates the number of oscillations (in space across a constant radius sphere) from $\theta = 0$ to π, just as the order n of a term in a Fourier analysis indicates the number of oscillations over the given interval from $x = 0$ to L.

Higher n means more wavelengths inside L. Higher l means more "wavelengths" inside 0 to π. (We use quotes on "wavelengths" in the spherical case, because (as we can see from the $l = 3$ case in (91)) a given l harmonic includes sub waves that oscillate less rapidly (e.g., the $l = 3$, $m = 0$ case of (91) has both a $\cos 3\theta$ and a $\cos\theta$ term, not just a $\cos 3\theta$ term).

<u>Question.</u> So, one might ask, if we could use either the complicated spherical harmonics or the simpler sines and cosines, why not analyze a spherical surface, like the LSS (last scattering surface) using the latter, rather than the former?

<u>Answer.</u> I believe it is for the following reasons.

> 1. We can convert readily between Fourier harmonic components in Cartesian coordinates (used to deduce conclusions about plane waves from inflation, etc.) and spherical harmonic components in spherical coordinates (in which our measurements are done) via the methodology of Sect. 3.3, pg. 7.

> 2. It is conventional.

> 3. Spherical harmonics are used elsewhere in physics, particularly in QM for the hydrogen atom wave function, and physicists are familiar with them. In the H atom case, we had no real choice but to use spherical harmonics, because they are eigenfunctions of the Schroedinger equation with the isotropic potential energy of the Coulomb potential of the nucleus. The eigenvalues of Y_{lm} are m and l (actually $l(l+1)$), which gave us respectively, the z direction angular momentum and the square of total angular momentum.

> 4. Spherical harmonics are eigenfunctions of any system having isotropic $g(\mathbf{x})$ in a governing equation like (54). Since one of the foundational postulates of modern cosmology is isotropy, in the long run, it should prove advantageous to represent quantities of interest in the universe (like wave patterns in the LSS) via eigenfunctions to equation (54) with isotropic $g = g(r)$.

> This would be particularly relevant for other cases involving 3D (unlike the 2D spherical surface of constant radius of the LSS). In such cases, we would have a non-trivial equation in r (see (59)), which is an eigenvalue problem with eigenvalue $l(l + 1)$. Thus, for each l (denoting a given eigenfunctions of r), there is a related eigenfunction of θ, <u>P_{lm}</u> (for given m). However, any given sine or cosine function, such as $\cos 3\theta$, is *not* an eigenfunction for given l.

> So, if we want to have the advantages of working in an eigenfunction basis for 3D isotropic cases, we need to use spherical harmonics, not sine/cosine functions.

11.5.5 An Example: A Dipole

Given that we align our spherical coordinate system (See Fig. A-2, pg. 27) in a given direction (say the z axis is aligned perpendicular to the plane of the galactic disk). One might realize that if there were a particular

multipole with respect to θ (particular l value) aligned with a node right on the z axis, then we could readily determine a suitable a_{lm}.
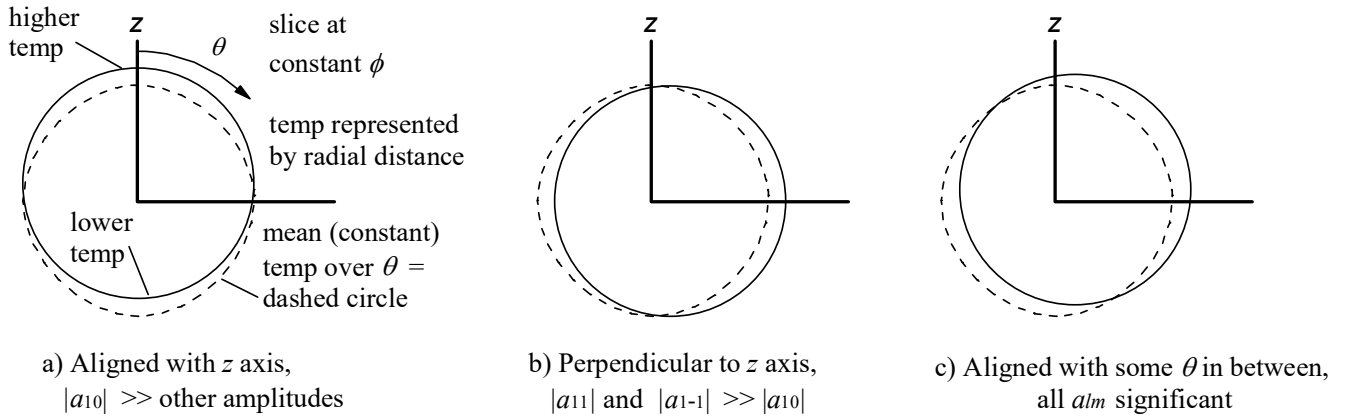
For example, consider the dipole of Fig. A-3, part a), aligned with the z axis. It is described, at least in large part, by a temperature variation with θ of $\cos\theta$. Note from (74), and (79),

$$T(\theta,\phi) = f(\theta,\phi) = \sum_{l=0}^{\infty} \sum_{m=-l}^{l} a_{lm} Y_{lm}(\theta,\phi) == \sum_{l=0}^{\infty} \sum_{m=-l}^{l} a_{lm} \sqrt{\frac{2l+1}{2}\frac{(l-m)!}{(l+m)!}} P_{lm}(\cos\theta) e^{im\phi} . \qquad (92)$$

From (65), we see the $l = 1$ terms include

$$P_{10} = \cos\theta \qquad P_{11} = -\sin\theta \qquad P_{1-1} = \tfrac{1}{2}\sin\theta \ . \qquad (93)$$

Higher order ($l > 1$) terms represent higher multipoles and $l = 0$ represents a constant (no multipole) value of temperature with respect to θ equal to 2.725°K for the CMB (see dashed circle in Fig. A-3). So we would expect the P_{10} term in the summation (92) to reflect the dipole of Fig. A-3a), i.e., a_{10} would be much larger than any other a_{lm}.

a) Aligned with z axis, $|a_{10}| \gg$ other amplitudes

b) Perpendicular to z axis, $|a_{11}|$ and $|a_{1-1}| \gg |a_{10}|$

c) Aligned with some θ in between, all a_{lm} significant

Figure A-3. Temperature Dipole Aligned in Three Different Directions

Similarly, in Fig. A-3b), the dipole is aligned such that the temperature variation, at least in large part, is described by $\sin\theta$. Thus, in that case, P_{11} and P_{1-1} would be the dominant contributing modes and be much larger than a_{10}. For the case of Fig. A-3c), we would have significant contributions from all three P_{lm}.

We now derive the a_{lm} for each of the cases in Fig. A-3 and see if our intuitive statements above regarding them are correct. To do this, we first note what the $l = 1$ part of the spherical harmonics summation looks like in general, where we look only at the slice where $\phi = 0$, to keep things simple for now.

General Relation for Dipole with Any Alignment

$$T_{l=1}(\theta,\phi) = \sum_{m=-1}^{1} a_{1m} Y_{1m}(\theta,\phi) = \sum_{m=-1}^{1} a_{1m} \sqrt{\frac{2+1}{2}\frac{(1-m)!}{(1+m)!}} P_{1m}(\cos\theta) \underbrace{e^{im\phi}}_{\substack{\text{take} \\ \phi=0}}$$

$$= a_{10}\sqrt{\frac{3}{2}\frac{(1)!}{(1)!}}\cos\theta - a_{11}\sqrt{\frac{3}{2}\frac{(0)!}{(2)!}}\sin\theta + a_{1-1}\sqrt{\frac{3}{2}\frac{(2)!}{(0)!}}\tfrac{1}{2}\sin\theta \qquad (94)$$

$$= a_{10}\sqrt{\frac{3}{2}}\cos\theta - a_{11}\frac{\sqrt{3}}{2}\sin\theta + a_{1-1}\frac{\sqrt{3}}{2}\sin\theta.$$

<u>Case of Fig A-3 a)</u>

For the first case in Fig. A-3, we have a simple cosine dependence on θ,

$$T_{l=1}(\theta,\phi) = X\cos\theta \qquad\qquad X = \text{max difference from mean temp .} \qquad (95)$$

So, in (94), we readily see that

$$a_{10} = \sqrt{\frac{2}{3}}X \qquad a_{11} = 0 \qquad a_{1-1} = 0 . \qquad (96)$$

<u>Case of Fig A-3 b)</u>

For the second case in Fig. A-3, we have a simple sine dependence on θ,

$$T_{l=1}(\theta,\phi) = X\sin\theta . \qquad (97)$$

The following satisfy (94) and are the a_{lm} values for the dipole as shown in Fig. A-3b).

$$a_{10} = 0 \qquad a_{11} = -\sqrt{\frac{1}{3}}X \qquad a_{1-1} = \sqrt{\frac{1}{3}}X . \qquad (98)$$

So,

$$T_{l=1}(\theta,\phi) = (0)\sqrt{\frac{3}{2}}\cos\theta + \frac{X}{\sqrt{3}}\frac{\sqrt{3}}{2}\sin\theta + \frac{X}{\sqrt{3}}\frac{\sqrt{3}}{2}\sin\theta = X\sin\theta . \qquad (99)$$

<u>Case of Fig A-3 c)</u>

For the third case of Fig. A-3, we have the following values, which we prove are correct below.

$$a_{10} = \frac{X}{\sqrt{3}} \qquad a_{11} = -\frac{X}{\sqrt{6}} \qquad a_{1-1} = \frac{X}{\sqrt{6}} , \qquad (100)$$

Note that the solid line of Fig. A-3c) is described by $X\sin(\theta+45°)$. From the trig relation

$$\sin(\alpha\pm\beta) = \sin\alpha\cos\beta \pm \cos\alpha\sin\beta \qquad \text{with } \alpha=\theta \text{ and } \beta = 45° , \qquad (101)$$

$$X\sin(\theta+45°) = X(\sin\theta\cos45° + \cos\theta\sin45°) = \frac{X}{\sqrt{2}}\sin\theta + \frac{X}{\sqrt{2}}\cos\theta . \qquad (102)$$

Using our stated values for the a_{lm} from (100) in (94), we see it equals (102). That is,

$$T_{l=1}(\theta,\phi) = \frac{X}{\sqrt{3}}\sqrt{\frac{3}{2}}\cos\theta + \frac{X}{\sqrt{6}}\frac{\sqrt{3}}{2}\sin\theta + \frac{X}{\sqrt{6}}\frac{\sqrt{3}}{2}\sin\theta = \frac{X}{\sqrt{2}}\sin\theta + \frac{X}{\sqrt{2}}\cos\theta , \qquad (103)$$

<u>A Comment</u>

I've tried to make this simple for illustrative purposes, but the astute reader may have noticed that the a_{11} and a_{1-1} are not uniquely defined above. Any of an infinite number of combinations of them could make (94) equal to (97) in Case b), or to (102) in Case c). Had we not limited this case to $\phi = 0$, in order to keep things simple, we could have shown they were actually unique for the more general case. See Sect. 11.5.3 pg. 33, where we show that, in general, for T to be real (not complex), we must have $a_{l-m} = (-1)^m a_{lm}^* = \text{real}$. This is a further constraint that pins down the a_{11} and a_{1-1} values. Note that (98) and (100) obey this constraint.

11.5.6 Other Multipoles

In similar fashion for a sole higher multipole (more spatial oscillations in temperature with θ = more "highs" and "lows" = more nodes = higher l value = l', for this example), the values for $a_{l'm}$ in the l' case would dominate over the a_{lm} values for other l.

In a general case with many multipoles superimposed (as in the CMB), we get a spectrum of a_{lm}, the values for each l and m reflecting how strong that particular mode is relative to all others in the summation (92).

The difficult thing about spherical harmonics, as seen by the examples of (65), is that it is not easy to visualize the various modes and what physically, exactly, their amplitudes a_{lm} represent. For a Fourier series like (90), we can envision what each mode looks like, and even draw figures representing the summations of the various modes. For spherical harmonics, on the other hand, this is problematic.

11.5.7 Angular Separation and *l*

From Fig. 3-A, pg. 36, one can see that for $l = 1$, there are 180° degrees between nodes, i.e., there is a single variation ("bump", as it were) over the range of $0 \le \theta \le \pi$. For $l = 2$, (think variation over 2θ, as in (91)) we would have three nodes (and two "bumps"), making a single variation (one "bump") over 90° degrees. For $l = 3$ (variation over 3θ as in (91)) we would have four nodes (three "bumps"), and a single variation (one "bump") over 60°. We can readily generalize to

$$\text{angular variation} = \frac{180°}{l} \quad \left(= \frac{\pi}{l} \text{ in radians} \right). \tag{104}$$

12 Appendix B. Introduction to Power Spectral Analysis

12.1 The Basis in Electronics for Power Considerations

Consider instantaneous power in an electric circuit

$$P_{inst} = VI , \tag{105}$$

where, for charge $q(t)$ a sinusoid, ω the frequency in radians/sec, and for simplicity impedance Z = pure resistance R,

$$q(t) = A\sin\omega t \qquad \left(A = q_{peak} \right)$$
$$I = \dot{q}(t) = \omega A\cos\omega t \qquad V = RI = R\omega A\cos\omega t \tag{106}$$

Thus, instantaneous power is

$$P_{inst} = R\omega^2 A^2 \sin^2\omega t = P_{peak}\sin^2\omega t \qquad P_{peak} = R\omega^2 A^2 \qquad \left(A = q_{peak} \right). \tag{107}$$

Since, for $T = 1/f = 2\pi/\omega$ the period of the oscillation,

$$\text{variance of } q = \frac{1}{T}\int_0^T \left(q(t) \right)^2 dt = \frac{1}{T}\int_0^T A^2\sin^2\omega t\, dt = \frac{1}{T}\int_0^T A^2 \left(\sin\frac{2\pi}{T}t \right)^2 dt = \frac{A^2}{2}$$

$$\text{standard deviation of } q = \sqrt{\text{variance}} = \text{rms value of } q = q_{rms} = \frac{A}{\sqrt{2}} , \tag{108}$$

the average power (time average of the instantaneous power) is

$$\underbrace{P = P_{mean}}_{\text{symbol def}} = \frac{1}{T}\int_0^T P_{inst}\, dt = \frac{1}{T}\int_0^T \underbrace{R\omega^2 A^2}_{P_{peak}}\sin^2\omega t\, dt = \frac{P_{peak}}{2} = R\omega^2 \frac{A^2}{2} \tag{109}$$

$$\frac{A^2}{2} \text{ is variance of } q(t) \quad \left(A = q_{peak} \right)$$

The point is the average power P is proportional to ω^2 times the amplitude of the charge squared A^2.

Now, for $q(t)$ a more general shape (non sinusoid), we can find the Fourier components of q, which when added together (or integrated in the continuous case), give us $q(t)$. The amplitude of each such component is, in

general, different at each value of ω, so we label such amplitudes as A_n (discrete case) or $A(\omega)$ (continuous case). That is,

$$q(t) = \sum_{n=0}^{\infty} \left(A_n \sin\omega_n t + B_n \cos\omega_n t \right) \quad \text{or} \quad q(t) = \int \left(A(\omega)\sin\omega t + B(\omega)\cos\omega t \right) dt \tag{110}$$

$$\text{take } B_n = B(\omega) = 0 \text{ for simplicity},$$

where we take the cosine parts to be zero, for simplicity, though to be complete for handling any shape $q(t)$, they would need to be included.

So, we would, in general, find a different average power P in (109) for each ω, and we define

$$P_n = \text{mean power for } n\text{th Fourier component in discrete case}$$
$$P(\omega) = \text{mean power per unit } \omega \text{ at } \omega \text{ in continuous case}, \tag{111}$$

In general, when people use the word "power" in the context of spectral analysis, they mean "mean power over a full cycle" as in (109) and (111), not instantaneous power, as in (107).

From (109), we can see that if our Fourier components A_n (or $A(\omega)$) of $q(t)$ had the same A_n (or $A(\omega)$) at each ω_n (or ω), the P_n data points (or the $P(\omega)$ curve) would rise quadratically with ω. A plot of $P(\omega)/\omega^2$ vs ω, on the other hand would be a straight line. See Fig. B-1.
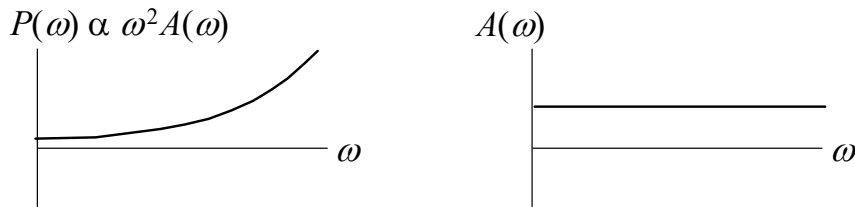
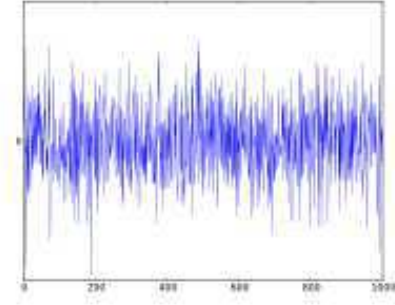

Figure B-1. Constant Amplitude $A(\omega)$

Intuitively, the behavior shown in Fig. B-1 could be expected. A sinusoidal wave of the same amplitude as another sinusoidal wave, but oscillating faster should have more power in it. Power depends on both the amplitude of the wave and the rate at which it oscillates.

White noise is defined as a straight line $P(\omega)$ vs ω curve, as shown in Fig. B-2 below. Each sinusoidal component at each ω has the same power density (power per unit ω), but as can be seen in the RHS of the figure, different amplitude $A(\omega)$.
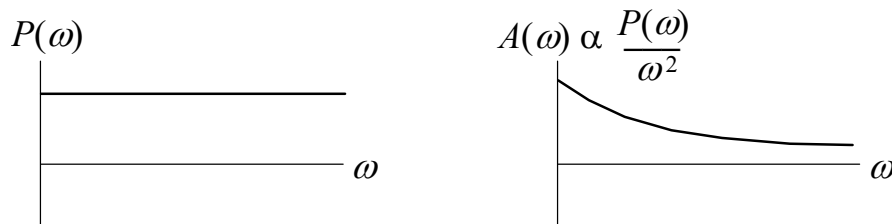
Figure B-2. White Noise = Constant $P(\omega)$

Fig. B-3 shows what white noise would look like in time, where the instantaneous contributions of every component of Fig. B-2 are summed as in (110) (actually, integrated for the continuous case of Fig. B-2) at each point in time.

Figure B-3. White Noise Instantaneous Power from All Components vs Time

More general type systems show varying behaviors, with plots that are more complicated than the ones above, but the relationship

$$P(\omega) \propto \omega^2 \frac{(A(\omega))^2}{2} \qquad A(\omega) = \text{amplitude of } \omega \text{ component wave} \qquad \frac{A(\omega)^2}{2} \text{ is variance of same wave} \quad (112)$$

always holds at each ω for any system.

12.2 Extrapolating to Other Types of Systems

The relations we developed in the prior section are commonly used for other fields outside of electronics. For spatially varying waves, for example, all of (105) to (111) can hold with different physical quantities, e.g.,

$$t \rightarrow x \qquad T \rightarrow \lambda \qquad q(t) \rightarrow S(x) \qquad \omega \rightarrow k \qquad A(\omega) \rightarrow A(k) \qquad P(\omega) \rightarrow P(k)$$
$$\lambda = \text{wavelength} \qquad S(x) = \text{any function of } x \qquad k = \text{wave number.} \tag{113}$$

For the CMB, we would take $S = T$, temperature (not period T as the symbol was used for above). And thus, we can immediately deduce, in parallel with (109), that

$$P(k) \propto k^2 \frac{(A(k))^2}{2} = k^2 \left\langle |A(k)|^2 \right\rangle$$

$$\frac{(A(k))^2}{2} = \left\langle |A(k)|^2 \right\rangle \text{ is variance of } k \text{ wave component of temperature } T(x) \tag{114}$$

$$\left(A(k) = T_{peak} \text{ for } k \text{ component} \right).$$

In this case, $P(k)$ vs k would be the temperature power spectrum. (Power is now being used in a more general, mathematical, sense, rather than being the kind of power one is accustomed to dealing with in mechanics and electronics. That is, power in the present sense does not have to be the time rate of change of work energy).

In the CMB analysis the above (Cartesian coordinates based) Fourier harmonics relationships are converted to (spherical coordinates based) spherical harmonics relationships, as shown in Sect. 6.

Note that units of $P(k)$ are power per unit k. When we integrate $P(k)$ over an interval Δk, we get the total power in that interval (a very useful relationship in many areas of physics and engineering).

$$\text{power between } k_1 \text{ and } k_2 = \int_{k_1}^{k_2} P(k) \, dk \tag{115}$$

Again, "power" in other contexts can mean something other than power as known in typical physics courses, and with other systems, such as that of (113), (115) holds with the surrogate symbols of (113) replacing those shown in (115).